Cell Systems

Report

Proteomics-Based Monitoring of Pathway Activity Reveals that Blocking Diacylglycerol Biosynthesis Rescues from Alpha-Synuclein Toxicity

Graphical Abstract

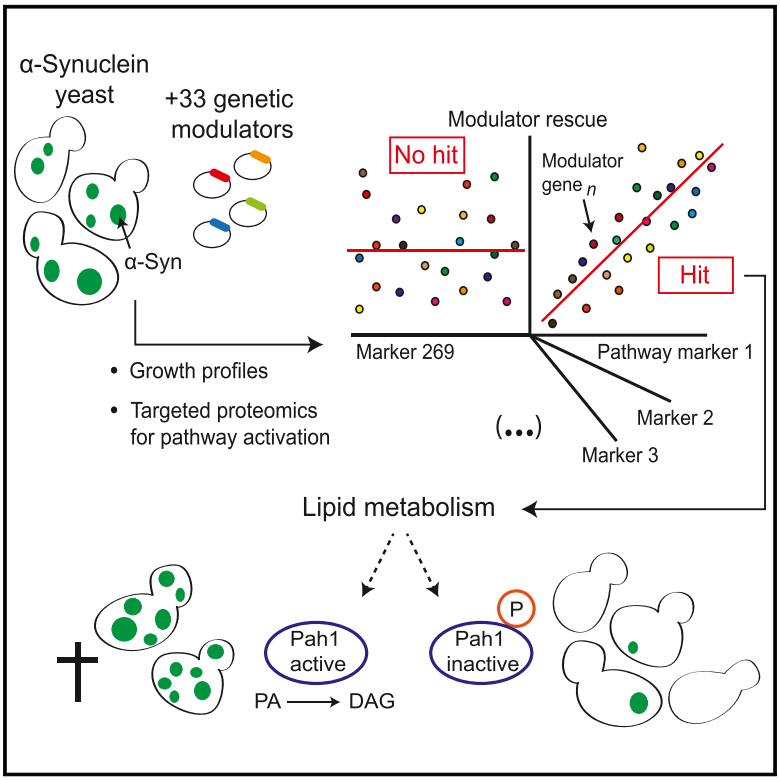

Highlights

- Proteomics of pathway sentinels across 33 genetic modulators of α-Synuclein toxicity
- Multidimensional linear regression predicts lipid metabolism to regulate rescue
- Genetic and chemical perturbation of Pah1 alters α-Synuclein inclusions and toxicity
- Diacylglycerol and lipid droplets may play a role in cytotoxicity induced by α-Synuclein

Authors

Martin Soste, Konstantina Charmpi, Fabienne Lampert, ..., Stefano Vanni, Andreas Beyer, Paola Picotti

Correspondence

andreas.beyer@uni-koeln.de (A.B.), picotti@imsb.biol.ethz.ch (P.P.)

In Brief

α-Synuclein is genetically and neuropathologically linked to Parkinson's disease. However, the mechanisms of known genetic toxicity modulators in a yeast model system remain largely unknown. In order to identify cellular rescue pathways at high-throughput, we have paired mass spectrometry-based monitoring of pathway activity and growth profiles through regression analysis. The results predicted a critical role for the protein Pah1 in lipid metabolism. Indeed, specific perturbation of Pah1 activity determines inclusion formation and toxicity thereby suggesting a potential target for combating pathologies associated with α-Synuclein accumulation.

Soste et al., 2019, Cell Systems 9, 309–320
September 25, 2019
https://doi.org/10.1016/j.cels.2019.07.010

CellPress

Cell Systems
Report

Proteomics-Based Monitoring of Pathway Activity Reveals that Blocking Diacylglycerol Biosynthesis Rescues from Alpha-Synuclein Toxicity

Martin Soste,[1,2,7] Konstantina Charmpi,[3,4] Fabienne Lampert,[1] Juan Atilio Gerez,[5] Marc van Oostrum,[1,8] Liliana Malinovska,[1,2] Paul Jonathan Boersema,[1,2] Natalia Cecilia Prymaczok,[5] Roland Riek,[5] Matthias Peter,[1] Stefano Vanni,[6] Andreas Beyer,[3,4,*] and Paola Picotti[1,2,9,*]

[1]Institute of Biochemistry, Department of Biology, ETH Zurich, Zurich, Switzerland
[2]Institute of Molecular Systems Biology, Department of Biology, ETH Zurich, Zurich, Switzerland
[3]CECAD, University of Cologne, Cologne, Germany
[4]Center for Molecular Medicine Cologne (CMMC), University of Cologne, Cologne, Germany
[5]Laboratory of Physical Chemistry, Department of Chemistry and Applied Biosciences, ETH Zurich, Zurich, Switzerland
[6]Department of Biology, University of Fribourg, Fribourg, Switzerland
[7]Present address: Donnelly Centre for Cellular and Biomolecular Research, University of Toronto, Toronto, Canada
[8]Present address: Institute of Molecular Systems Biology, Department of Biology and Biomedical Proteomics Platform, Department of Health Sciences and Technology, ETH Zurich, Zurich, Switzerland
[9]Lead Contact
*Correspondence: andreas.beyer@uni-koeln.de (A.B.), picotti@imsb.biol.ethz.ch (P.P.)
https://doi.org/10.1016/j.cels.2019.07.010

SUMMARY

Proteinaceous inclusions containing alpha-synuclein (α-Syn) have been implicated in neuronal toxicity in Parkinson's disease, but the pathways that modulate toxicity remain enigmatic. Here, we used a targeted proteomic assay to simultaneously measure 269 pathway activation markers and proteins deregulated by α-Syn expression across a panel of 33 *Saccharomyces cerevisiae* strains that genetically modulate α-Syn toxicity. Applying multidimensional linear regression analysis to these data predicted Pah1, a phosphatase that catalyzes conversion of phosphatidic acid to diacylglycerol at the endoplasmic reticulum membrane, as an effector of rescue. Follow-up studies demonstrated that inhibition of Pah1 activity ameliorates the toxic effects of α-Syn, indicate that the diacylglycerol branch of lipid metabolism could enhance α-Syn neuronal cytotoxicity, and suggest a link between α-Syn toxicity and the biology of lipid droplets.

INTRODUCTION

Alpha-synuclein (α-Syn) is an aggregation-prone protein implicated in Parkinson's disease (PD). Insoluble α-Syn species are a major component of Lewy bodies, which are proteinaceous inclusions found in post-mortem analyses of PD patient brains (Spillantini et al., 1997). Amplification and mutations in the gene encoding α-Syn result in dominant familial parkinsonism (Polymeropoulos et al., 1997; Singleton et al., 2003). α-Syn is a soluble, cytoplasmic protein that can bind to certain lipids and cellular membranes (Snead and Eliezer, 2014). These interactions appear to be important for the normal function of α-Syn and may also play roles in the aggregation of the protein into cytoplasmic inclusions, but the precise molecular events underlying α-Syn neuronal toxicity remain elusive.

The proteotoxicity of α-Syn has been modeled in a variety of systems (Fares et al., 2016; Khurana and Lindquist, 2010; Luk et al., 2012), including *Saccharomyces cerevisiae* (Outeiro and Lindquist, 2003), resulting in translatable findings (Chung et al., 2013; Tardiff et al., 2013). In yeast, ectopically expressed α-Syn forms intracellular inclusions and causes dose- and time-dependent cytotoxicity (Outeiro and Lindquist, 2003). Genome-wide screens performed in yeast have identified dozens of genes that upon overexpression or silencing modulate toxicity (Cooper et al., 2006; Gitler et al., 2009; Khurana et al., 2017; Willingham et al., 2003; Yeger-Lotem et al., 2009). The human homologues of several conserved yeast genes from this set, such as *RAB1* and *NEDD4* (Chung et al., 2013; Cooper et al., 2006), modulate α-Syn toxicity in neuronal cells, and mutations in another identified gene *ATP13A2* (also known as *PARK9*) cause an autosomal recessive form of PD (Gitler et al., 2009; Ramirez et al., 2006). Despite these promising findings and the agreement across species, the molecular mechanisms of genetic modifiers of α-Syn toxicity are largely unknown.

In this study, we sought to systematically identify pathways and biological processes that act downstream of genetic modifiers of α-Syn toxicity. We used a recently developed proteomics approach that enables simultaneous monitoring of activation states of a variety of biological processes (Soste et al., 2014). This approach is based on quantitative detection of sentinel proteins, which are biological markers that change in abundance or phosphorylation state or are cleaved at specific sites in response to changes in activity of the associated pathway. Examples of sentinels are levels of Atg8 or cleavage of Ape1, which are

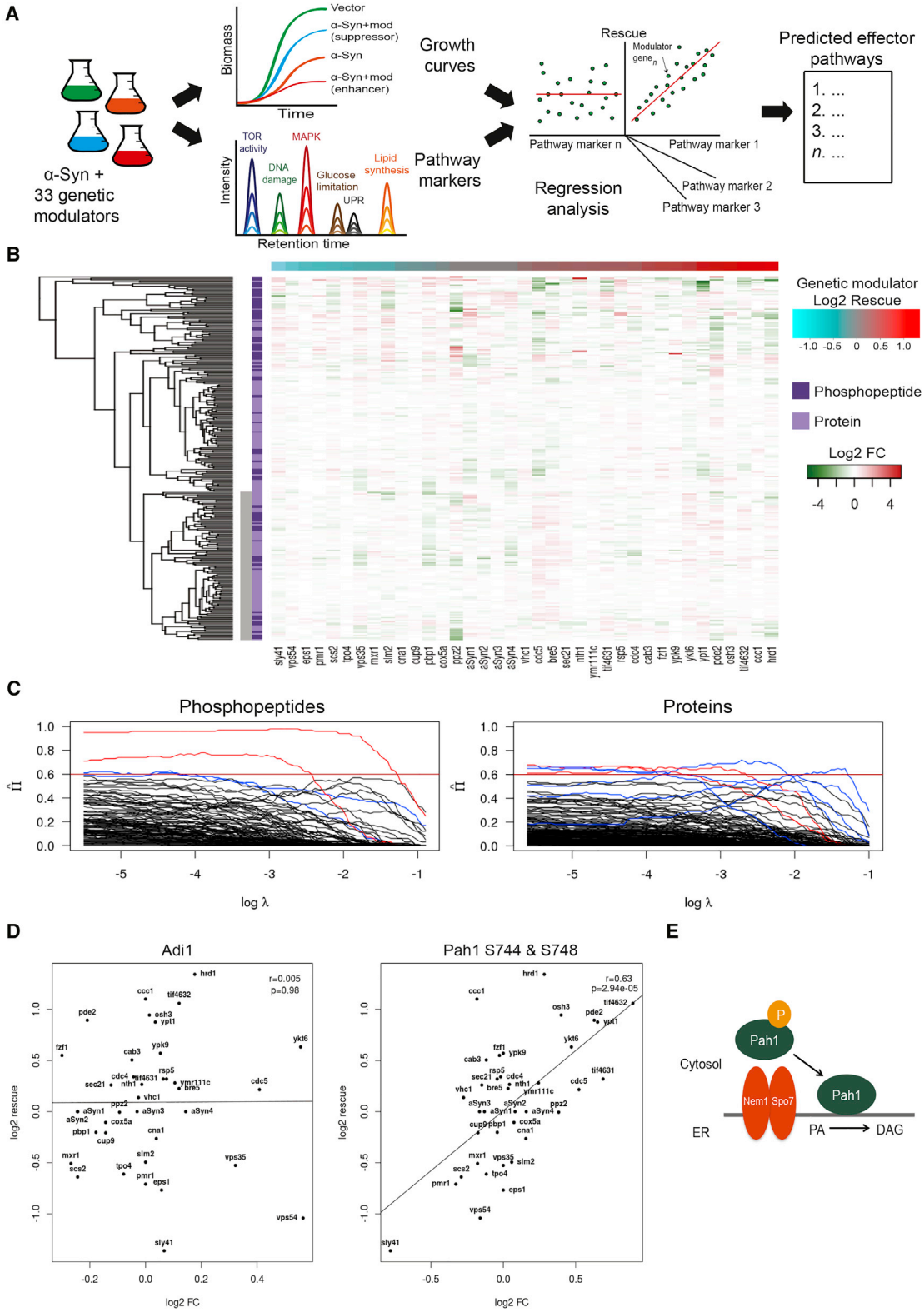

Figure 1. Relating Growth and Pathway Activation Data through Regression Analysis to Identify Effectors of Rescue from α-Syn-Induced Toxicity

(A) Workflow to predict cellular pathways that rescue yeast from α-Syn-induced toxicity. Mod, α-Syn genetic modulator.

(B) Sentinel quantification for each α-Syn genetic modulator. Genetic modulators are ordered in columns according to their genetic modulation effect from enhancement of toxicity (blue) to suppression of toxicity (red). aSyn, α-Syn expression without genetic modulation. Phosphopeptide (dark purple) and protein

(legend continued on next page)

indicators of activation of autophagy (Klionsky, 2007; Suzuki et al., 2002), and phosphorylation of MAP kinases that mark activation of this pathway (Cherkasova, 2006).

As sentinels of α-Syn-mediated toxicity, we monitored 269 total markers: 178 sentinels report the activation states of 140 biological processes and 91 sentinels that were selected from shotgun proteomic analyses of α-Syn-perturbed yeast or prior knowledge about α-Syn biology. We analyzed genetically engineered strains that simultaneously express α-Syn and one of 33 different α-Syn genetic modulators. In order to identify pathways that rescue cells from α-Syn-mediated toxicity, we employed a multiple linear regression approach, which implicated Pah1, a phosphatase that catalyzes conversion of phosphatidic acid to diacylglycerol at the endoplasmic reticulum (ER), as an effector of rescue. Thus, a lipid biosynthetic pathway is a potential instrument for amelioration of α-Syn-induced pathology.

RESULTS

Proteome Responses to α-Syn Toxicity in Yeast

α-Syn pathobiology can be modeled in yeast by inducible expression of human α-Syn (Outeiro and Lindquist, 2003). Expression of a single α-Syn copy results in its localization to the plasma membrane with no appreciable toxicity, whereas expression of two copies leads to the formation of large cytoplasmic inclusions and inhibition of yeast growth. We performed shotgun proteomics and phosphoproteomics analyses at 6 h post-induction of expression of two copies of α-Syn and of vector control. α-Syn intracellular inclusions were detected in the α-Syn-expressing cells and while growth rate was reduced compared to control cells, α-Syn-expressing cells remained viable (Figures S1A–S1C). In total, 3,679 proteins and 5,464 phosphopeptides were quantified using a label-free proteomics approach. Levels of 160 proteins and 228 phosphopeptides were significantly different in α-Syn-expressing cells compared to control (fold change $\geq$ 2, q $\leq$ 0.01, Figures S1D–S1G; Table S1).

Functional enrichment analyses of regulated proteins and phosphoproteins based on gene ontology (GO) terms and Munich Information Center For Protein Sequences (MIPS) categories revealed differential expression of AGC protein kinase-encoding genes and genes involved in the vacuole, the ER, and the plasma membrane (Table S2), three subcellular locations known to be affected by α-Syn (Gitler et al., 2009; Petroi et al., 2012). Next, we asked whether proteins upregulated in α-Syn-expressing cells were toxic when expressed beyond a certain level by cross-referencing a previously reported dataset (Makanae et al., 2013). Four significantly upregulated proteins (Erg2, Erg25, Nce102, and Vma3) are encoded by dosage-sensitive genes, suggesting that α-Syn toxicity could be linked to increased expression of these genes. Of 102 proteins previously shown to be associated with rescue from α-Syn toxicity (Khurana et al., 2017; Yeger-Lotem et al., 2009), 62 were identified in our screen, and three of these (Cmc2, Pan2, and Osh2) were significantly upregulated (Table S1, red). Upregulation of these genes could counteract toxicity of α-Syn (Cooper et al., 2006; Gitler et al., 2009).

Identification of Pathways that Rescue from α-Syn Toxicity Using an Expanded Sentinel Assay

The sentinel assay previously developed by our group quantified 202 (phospho)proteins that report known pathway activation events in response to well-characterized perturbations (Soste et al., 2014). We reasoned that monitoring the extent of activation of these pathways in response to expression of genetic modulators of α-Syn toxicity would provide a comprehensive view of their cellular effects. As α-Syn may trigger molecular events not captured by our original assay, we expanded it to include 33 proteins and 66 phosphopeptides that either reacted to the overexpression of α-Syn and were prioritized based on amplitude of response, known functions, and conservation in humans or were previously linked to α-Syn. In the latter set, we included sentinels for a phosphorylation site and three ubiquitination sites on α-Syn since these modifications were implicated in toxicity (Oueslati et al., 2010, 2012) and a marker for the degradation of Cpy1, which has been used as a reporter for an α-Syn-induced vesicle trafficking defect (Cooper et al., 2006). We developed targeted quantitative proteomics assays based on parallel reaction monitoring (PRM) mass spectrometry for these proteins (Tables S3 and S4).

The expanded sentinel assay was used to analyze effects of 33 genetic modulators of α-Syn identified through previous screens and hypothesis-driven studies (Cooper et al., 2006; Gitler et al., 2009; Khurana et al., 2017; Tardiff et al., 2013; Yeger-Lotem et al., 2009) (Figure 1A; Table S5). We expressed each genetic modulator together with α-Syn, both under control of a galactose-inducible promoter. After 6 h, we monitored pathway activation. We also quantified the extent of rescue or toxicity enhancement achieved by expression of each genetic modulator compared to cells that did not express the modulator by quantitative analyses of growth curves.

We quantified a total of 269 sentinels per genetic modulator (Figure 1B; Table S6). This consisted of 178 generic pathway

(light purple) pathway sentinels are hierarchically clustered in rows. Log_2 fold-change (FC) in sentinel abundance relative to vector strain is shown on a color scale of green (decreased) to red (increased). Gray bar denotes cluster of oppositely regulated sentinels. See also Tables S6, S7, and S8.

(C) Regression analysis of pathway sentinels and genetic rescue using stability selection in order to identify strongest predictors of rescue. Selection probability ($\hat{\Pi}$) plotted as a function of the regularization parameter (λ) displays stability paths of phosphopeptides (left) and proteins (right). Sentinels that passed the cutoff of selection probability (horizontal red line, 0.6) after fitting a multiple linear regression model are colored: red paths indicate a positive association with rescue, and blue paths indicate a negative association. Corresponding selected pathway sentinels are shown in Table S12.

(D) Correlation plots for two sentinel proteins, Adi1 and Pah1. Plots show the extent of rescue relative to the unmodulated α-Syn strain and report on the respective cellular process, heat-shock response and lipid metabolism, as monitored by FC of an Adi1 peptide and the Pah1 peptide containing phosphorylation sites S744 and S748 relative to the vector strain. r, Pearson correlation coefficient. p, p-value from application of the correlation test (n = 37).

(E) Schematic of the role of Pah1 in lipid metabolism. Pah1 is dephosphorylated by the Nem1-Spo7 complex to catalyze conversion of PA into DAG. P, Phosphorylation.

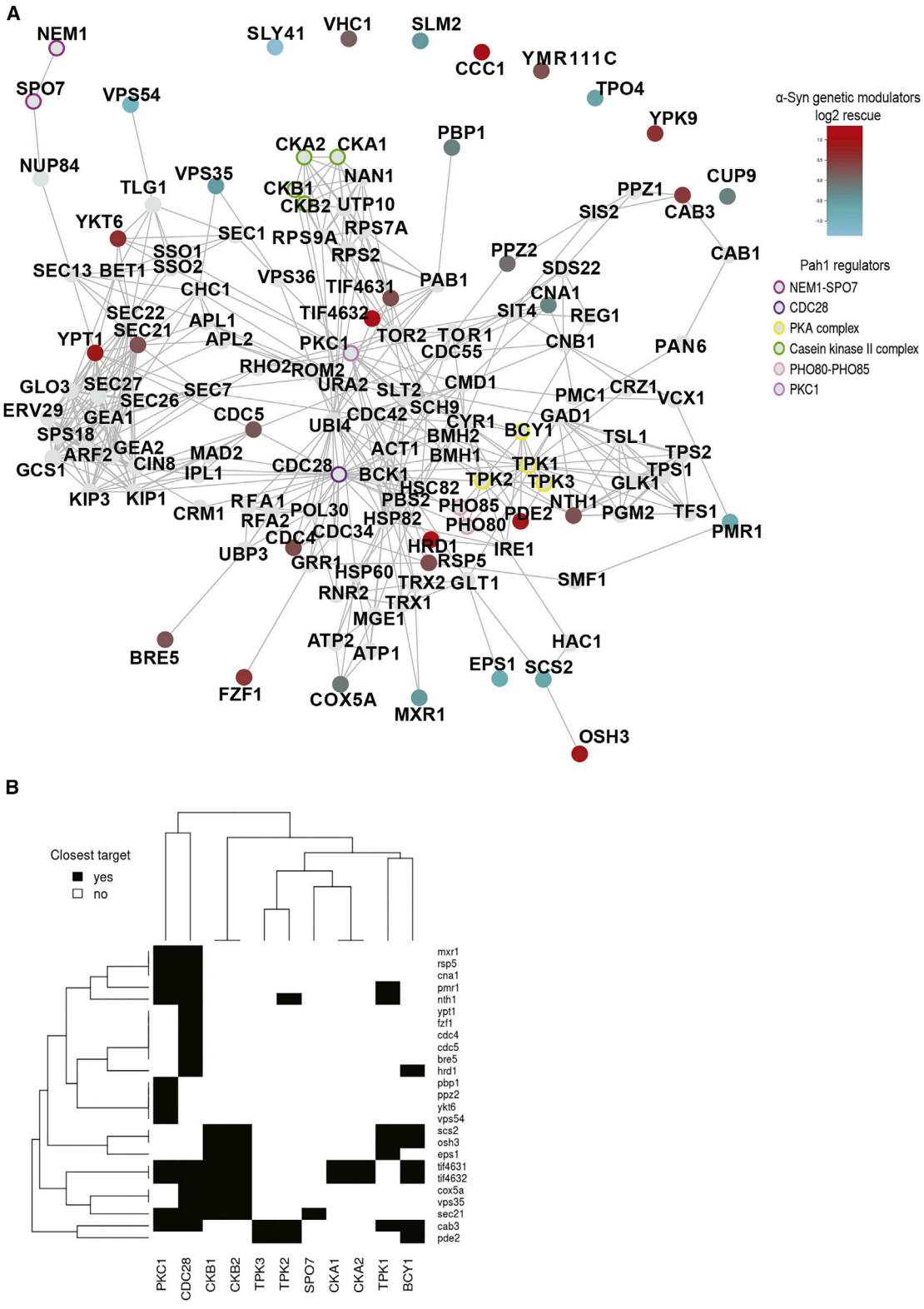

Figure 2. Network Paths Connecting α-Syn Genetic Modulators to Known Regulators of Pah1

(A) A subgraph of nodes included in the shortest paths between α-Syn genetic modulators and their closest target among known Pah1 regulators (Nem1-Spo7, Cdc28, PKA complex, casein kinase II complex, Pho80-85, Pkc1) was obtained using the STRING *Saccharomyces cerevisiae* network. Genetic modulators are

(legend continued on next page)

markers (140 biological processes) and 91 α-Syn-specific markers, made up of 103 phosphopeptides and 166 proteins. In 88% of cases, expression of genes expected to ameliorate α-Syn-mediated toxicity or to increase toxicity matched findings from previous genetic screens (Figure S1H; Table S7). Clustering based on the similarities of sentinel profiles, revealed that modulators involved in the same cellular process generally grouped together (Figure S1I) and that modulators from related processes (e.g., endocytosis and vesicle transport) clustered in proximity. Thus, closely related modulators induce similar downstream effects. The mean Pearson correlation coefficient (r) and the coefficient of determination (R^2) for sentinel abundances from replicated analysis of unmodulated α-Syn strains were 0.92 and 0.85 for proteins and 0.78 and 0.61 for phosphopeptides, respectively (Figure S1J). We also identified 100 proteins that were oppositely regulated upon expression of genetic enhancers versus genetic suppressors of toxicity (Figure 1B, gray bar, Table S8) that were enriched for processes previously attributed to α-Syn toxicity such as oxidative stress and protein folding (Table S9).

Next, we identified pathways that best correlated with the extent of rescue based on the abundances of the respective sentinels. Rather than individually correlating the state of each sentinel with rescue of the yeast strain, we used a regularized multiple regression approach that accounted for the fact that multiple pathways together might best explain the phenotypic rescue. We applied sparse linear regression analyses based on lasso with stability selection (Meinshausen and Bühlmann, 2010) (see STAR Methods, Figure 1C; Tables S10 and S11). For the majority of proteins and pathways we found no correlation between the extent of rescue and abundance of the associated sentinel (Figure 1D; left, Figures S2A and S2B). Correlations were observed for some sentinels (Figure S2C); however, only four phosphoprotein sentinels (Pah1, Num1, She3, and Osh1) and seven protein sentinels (Met10, Ncp1, Car1, Dot5, Gpp1, Ero1, and Cwp1) were predictive of rescue with a selection probability greater than or equal to 60% (Figure 1C, red and blue, Figure S2D; Table S12). These markers are involved in lipid, sterol, and amino acid metabolism, mitochondria-ER-cortex-anchoring, cell-wall biosynthesis, mRNA transport, cortical ER inheritance, oxidative stress, and protein folding. Biological processes associated with sentinels that correlated with rescue included vesicle-trafficking defects, which were previously shown to be involved in α-Syn toxicity (Cooper et al., 2006). Vesicle trafficking was monitored in our assay by the ER-to-Golgi trafficking of the protein Cpy1, which had a selection frequency below 60% but ranked 12th of 166 protein sentinels (Table S11). This indicates that our method captured meaningful biological events associated with α-Syn toxicity.

The top ranked pathway sentinel was phosphorylation of the protein Pah1, a marker for the biosynthesis of diacylglycerol (DAG) (Figure 1D, right, Figure S2D; Table S12). Dephosphorylation of Pah1 by the Nem1-Spo7 complex is known to activate the enzyme (O'Hara et al., 2006; Su et al., 2014). Activated Pah1 catalyzes the conversion of phosphatidic acid (PA) to DAG at the ER membrane; inactive Pah1 is localized to the cytosol (Hsieh et al., 2016) (Figure 1E). Our data indicate that phosphorylation, and therefore inactivation, of Pah1 positively correlates with rescue from α-Syn toxicity and suggests that Pah1 may act downstream of a broad range of α-Syn genetic modulators.

Network Paths Linking Genetic Modulators to Pah1

Overexpression of several genetic modulators of α-Syn toxicity resulted in the regulation of Pah1 phosphorylation. To assess how diverse genetic modulators are linked to Pah1 phosphorylation, we performed network analyses using the tool, STRING (Szklarczyk et al., 2019). We searched in the high-confidence STRING yeast protein association network for the shortest paths between each genetic modulator and six known upstream regulators of Pah1 (Nem1-Spo7, Cdc28, PKA complex, CK2 complex, Pho80-Pho85, and Pkc1) (Figure 2A). In the resulting subnetwork, 25 genetic modulators were linked to Pah1 regulators whereas eight were not. Shortest path analysis revealed common and disparate downstream paths connecting modulators and Pah1. Modulators known to be involved in the same biological process grouped together in the Pah1 network. Modulators that induced the largest fold changes in Pah1 phosphorylation were direct neighbors or within two edges of a known Pah1 regulator (Figure S2E). For example, the modulators *TIF4631*, *TIF4632*, and *YKT6* are within two edges of the known regulator Pkc1, which phosphorylates Pah1 to stimulate its proteasomal degradation (Hsieh et al., 2015). Modulators *PDE2* and *HRD1* are within two edges of the PKA complex, which has the opposite effect on Pah1 proteasomal degradation and attenuates its catalytic activity (Su et al., 2012). *YPT1* and *CDC5* are within two edges of Cdc28, which has not been found to affect Pah1 catalytic activity but does phosphorylate Pah1 and potentially influences its localization (Hsieh et al., 2016). For some modulators, more than one Pah1 phosphorylation regulator was equally close (i.e., there were multiple paths of the same length) (Figure 2B; Table S13). 40% of modulators were closest to a single Pah1 regulator, 36% were equidistant to two regulators, and 24% were equidistant to three or four. The most central nodes in the network were Cdc28, Ubi4, Ura2, Tpk1, and Pkc1 (Table S13).

Deletion of *NEM1* Increases Levels of Phosphorylated Pah1 and Suppresses α-Syn Toxicity

We next assessed whether Pah1 phosphorylation is sufficient to ameliorate α-Syn-mediated toxicity. First, we deleted the gene encoding the phosphatase Nem1, which is responsible for dephosphorylation of Pah1 at the two residues identified in our screen and five other residues (Santos-Rosa et al., 2005). The α-Syn-expressing Δ*nem1* strain grew better than the α-Syn-expressing strain without the deletion, suggesting that phosphorylation of Pah1 promotes cellular fitness in the presence of high levels of α-Syn (Figure 3A). To confirm that phosphorylation of Pah1 was indeed increased in the α-Syn-expressing Δ*nem1*

colored by a blue to red gradient according to their rescue effect; known Pah1 regulators are colored rings and discovered intermediate nodes are shown in gray. The known Pah1 regulators are 14 proteins involved in six complexes; complex members have matched colors.
(B) The closest Pah1 regulator of each modulator is shown (black cell). If more than one Pah1 regulator had the same shortest distance from a genetic modulator, then multiple Pah1 regulators were designated as closest. See also Table S13.

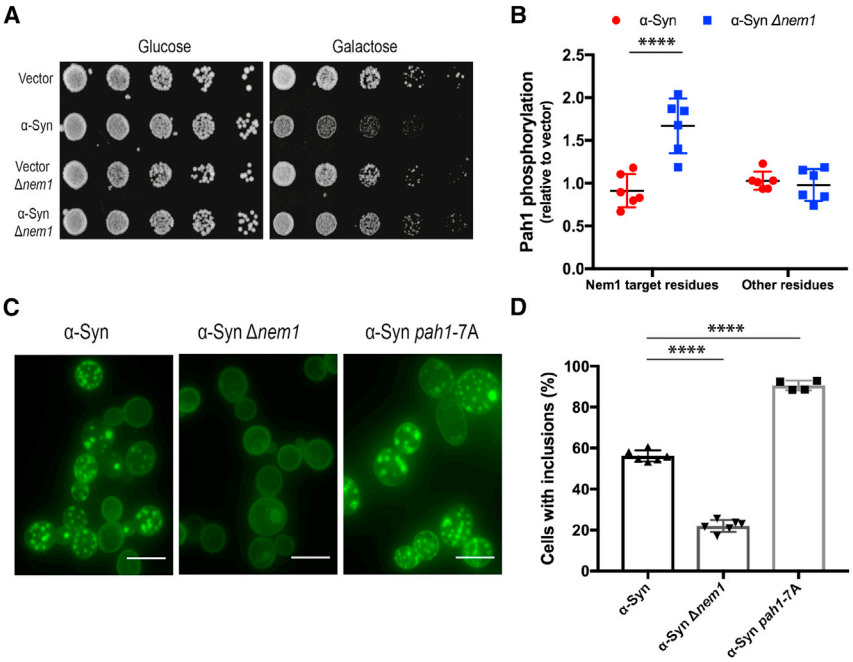

Figure 3. Deletion of *NEM1* Suppresses Toxicity Caused by α-Syn Expression and Alters Inclusion Phenotype

(A) Cultures of indicated yeast strains spotted by serial dilution onto glucose and galactose-containing medium. α-Syn expression is under the control of a galactose-inducible promoter.

(B) Pah1 phosphorylation levels assessed by targeted proteomic measurement of two phosphopeptides containing three known Nem1-target sites and two phosphopeptides with two residues not targeted by Nem1. See also Table S14. Mean ± standard deviation abundances for two peptides in each group (Nem1 target residues and other residues) in biological triplicates were compared (two-way ANOVA adjusted for multiple comparisons, n = 6, alpha = 0.05).

(C) Representative images of cells that express α-Syn-YFP and mutants with opposite effects on Pah1 phosphorylation status. Scale bars represent 10 μm. See also Figure S3E.

(D) Cells with and without α-Syn-YFP inclusions were counted in three fields of view. The mean counts expressed as percentages ± standard deviation of biological replicates were compared (one-way ANOVA adjusted for multiple comparisons, n > 3, alpha = 0.05). ****, p < 0.0001.

strain, we measured phosphorylation of Pah1 by targeted mass spectrometry. As expected, Pah1 phosphorylation at known Nem1 target sites, and not at other residues, was significantly increased in the absence of the Nem1 phosphatase (Figure 3B). Of note, no Δ*nem1*-induced suppression of toxicity was observed in cells expressing aggregation-prone proteins TDP-43 and FUS, indicating that the effect is specific to α-Syn (Figure S3A). Western blot analyses showed that mutants that resulted in Pah1-related rescue or enhanced toxicity did not affect α-Syn expression (Figure S3B). Collectively, these data confirm the prediction resulting from our sentinel analysis that Pah1 phosphorylation specifically counteracts the toxic effects of α-Syn.

The Diacylglycerol Branch of Lipid Metabolism Enhances α-Syn Toxicity

α-Syn inclusions are a hallmark of toxicity in the yeast model and are associated with lipids and neutral lipid droplets in yeast and mammalian cells (Cole et al., 2002; Outeiro and Lindquist, 2003). Pah1 controls the formation of cytosolic lipid droplets by catalyzing the biosynthesis of DAG, and cells with abrogated Pah1 activity have fewer droplets than control cells (Adeyo et al., 2011). To determine whether modulation of Pah1 affects α-Syn inclusions, we first established that α-Syn binds lipids in our model by demonstrating co-localization of YFP-tagged α-Syn with Nile red-positive lipids (Figures S3C and S3D). Next, we imaged YFP-tagged α-Syn in the Δ*nem1* strain and in the strain expressing *pah1*–7A, a mutant with higher than wild-type activity (Choi et al., 2011; O'Hara et al., 2006). We found that there were significantly fewer cells with large α-Syn inclusions in the Δ*nem1* strain and significantly more in the *pah1*–7A strain relative to the control strain (Figures 3C, 3D, and S3E). There were fewer inclusions in the Δ*pah1* strain and in the strain in which *PAH1* was replaced with the catalytically inactive mutant *pah1*-D398E than in the control strain (Figures S3F and S3G) (Han et al., 2007). Despite modulation of toxicity by deletion of *NEM1* or expression of *pah1*–7A, we observed co-localization of α-Syn with Nile red-positive lipids (Figures S3C and S3D), and there were fewer lipids in Δ*nem1* cells and more lipids in *pah1*–7A α-Syn-expressing cells than in wild-type cells that expressed α-Syn (Figure S3H). In summary, these data show that α-Syn inclusion formation depends on activation of Pah1.

To confirm that the phosphorylation status of Pah1 has an effect on toxicity, we assayed growth of the *pah1*–7A strain. The growth of yeast perturbed by both α-Syn and *pah1*–7A expression was significantly lower than expected based on each perturbation alone (Figure 4A), indicating a synergistic interaction between the 7A mutant of Pah1 and α-Syn expression (Figure 4B). The 7D/E phospho-mimic of Pah1 did not decrease the number of cells with inclusions or rescue growth relative to cells that expressed wild-type Pah1 (Figures S3G, S3I, and S3J). A possible explanation is that this phospho-mimic does not have the same effect as endogenous phosphorylation, a phenomenon known to occur (Paleologou et al., 2008). Since Δ*pah1* and *pah1*-D398E strains were more resilient than expected to the toxic effects of α-Syn there appears to be an alleviating interaction between these mutations and α-Syn (Figure 4B). This analysis of *PAH1* mutants further supported our hypothesis that Pah1 deactivation promotes rescue.

Deactivation of Pah1 results in decreased DAG levels, but also in accumulation of PA and, consequently, expression of genes known to be associated with phospholipid biosynthesis (Figure 4C) (Henry et al., 2012; White et al., 1991). We hypothesized that rescue resulted from upregulation PA rather than a decrease in the levels of DAG. We tested this possibility by growing α-Syn-expressing yeast cells in inositol, which decreases production of PA and thus inhibits phospholipid gene expression. If this pathway was the rescue mechanism, we would expect enhanced toxicity in the presence of inositol, but we found that inositol treatment did not enhance toxicity (Figure 4D),

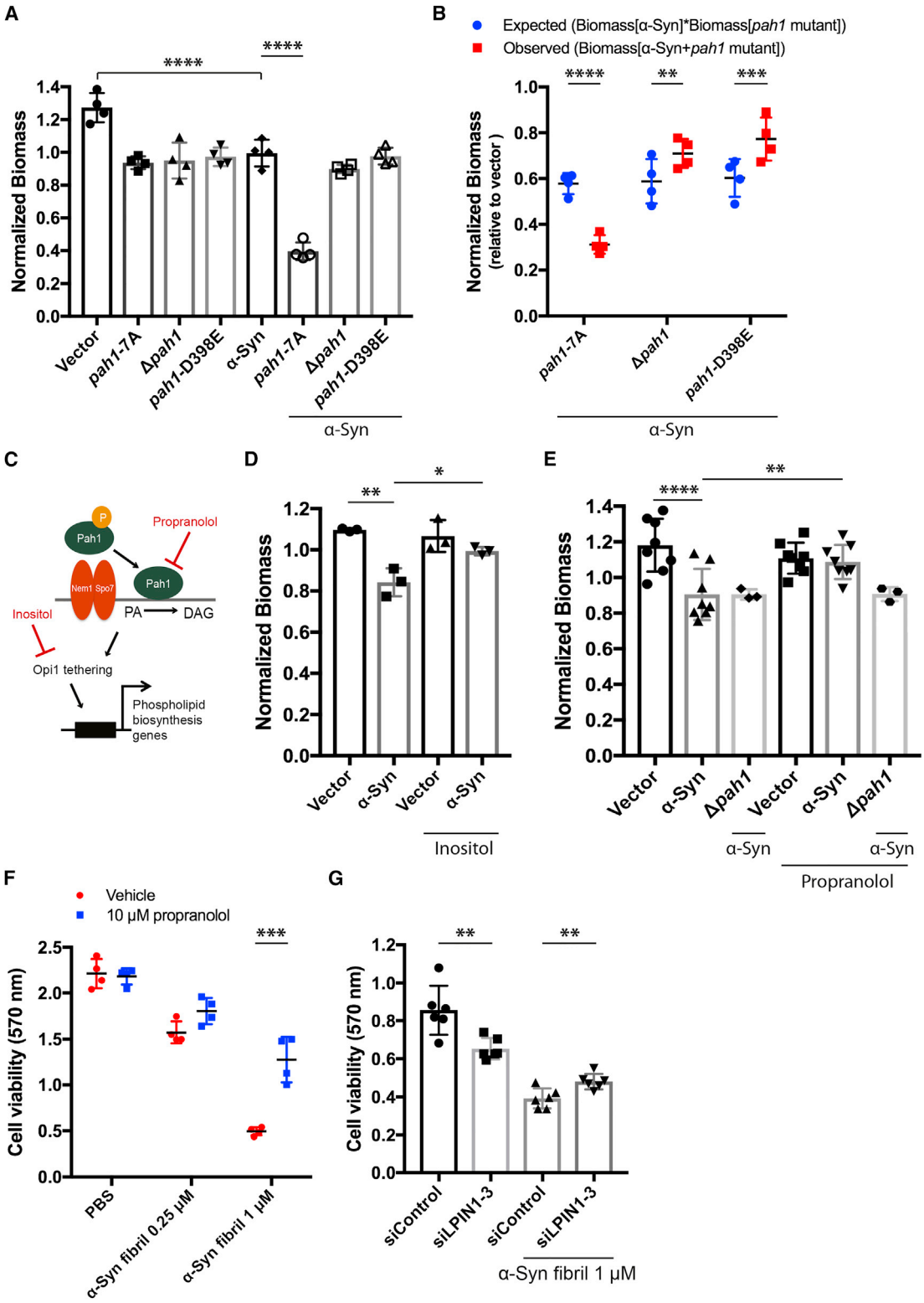

Figure 4. Pah1 Activity in the DAG Branch of Lipid Metabolism Regulates α-Syn Toxicity in Yeast and Mammalian Cells

(A) Biomass of *PAH1* mutant-expressing yeast strains grown with or without 1 nM estradiol to induce α-Syn expression were monitored over 24 h. Light scattering (620 nm) measurements were baselined on a well-by-well basis, summed, and divided by mean replicate intensity to obtain normalized biomass values (one-way ANOVA adjusted for multiple comparisons, n = 4, alpha = 0.05).

(legend continued on next page)

suggesting that the reduction in DAG biosynthesis rather than accumulation of PA is relevant to the resistance of cells to α-Syn-mediated toxicity.

Chemical Inhibition of Pah1 Activity Suppresses α-Syn Toxicity in Yeast and Mammalian Cells

To determine whether chemical inhibition of Pah1 would protect cells from α-Syn-induced toxicity, we treated α-Syn-expressing yeast cells with the well-characterized Pah1 inhibitor propranolol (Morlock et al., 1991). By monitoring biomass over 24 h, we found that 2 mM propranolol significantly suppressed toxicity in a Pah1-dependent manner (Figure 4E). This result further supports our conclusion that Pah1 activity promotes α-Syn toxicity through the conversion of PA to DAG.

To determine whether lipins (*LPIN1/2/3*), the mammalian homologs of *PAH1*, modulate α-Syn toxicity in neuronal cells, we treated mouse neuroblastoma N2A cells with fibrils pre-formed from recombinant α-Syn in the presence and absence of propranolol and assayed for cell viability. We chose this model of α-Syn toxicity because it better recapitulates PD hallmarks such as accumulation of intracellular α-Syn inclusions and neuronal toxicity than do models based on the intracellular neuronal expression of α-Syn (Gerez et al., 2019; Luk et al., 2009, 2012; Theillet et al., 2016). Administration of α-Syn fibrils to N2A cells induced toxicity in a dose-dependent manner (one-way ANOVA, $p < 0.0001$). At the highest dose of administered α-Syn fibrils, cell viability was significantly increased by treatment with 10 μM propranolol (Figure 4F). In order to characterize the effects of propranolol, we conducted a shotgun phosphoproteomic analysis of α-Syn-expressing yeast cells with and without propranolol treatment. We found that the Pah1 network was affected by propranolol treatment, although various other phosphoproteins unrelated to Pah1 were also regulated (Figure S4A; Table S15). Finally, we silenced all three *LPIN* genes in HEK293 cells treated with α-Syn fibrils (Figure S4B). Treatment with α-Syn fibrils alone or silencing of *LPIN* genes alone both decreased viability of HEK293 cells; however, toxicity of α-Syn fibrils was decreased in cells in which all three *LPIN* genes had been silenced compared to control cells (Figure 4G). Overall, these results confirm our findings in yeast and indicate that inhibition of lipin activity or silencing of *LPIN* genes suppresses toxicity of α-Syn fibrils in mammalian cells.

DISCUSSION

α-Syn plays a crucial role in Parkinson's disease (Polymeropoulos et al., 1997; Singleton et al., 2003), but the mechanisms that underlie this toxicity have remained cryptic making development of effective therapies challenging. In this study, we simultaneously measured activation states of a multitude of pathways and levels of proteins that are deregulated by expression of α-Syn across a diverse set of known genetic modulators of α-Syn toxicity. We applied multidimensional linear regression analysis to identify biological processes that correlated with the rescue from toxicity. Pah1 phosphorylation, which inhibits its activity, was predicted to protect cells from the toxic effects of α-Syn.

α-Syn expression in yeast results in lipid droplet (LD) accumulation (Outeiro and Lindquist, 2003; Sere et al., 2010), and α-Syn inclusions co-localize with LDs (Cole et al., 2002; Wang et al., 2013). Our data show that Pah1 inhibition, which antagonizes LD formation and lipid storage by halting DAG production (Barbosa et al., 2015), ameliorates α-Syn-mediated toxicity and results in the reduction of α-Syn inclusion formation, suggesting tight links between α-Syn-mediated toxicity, lipid metabolism resulting in DAG production, and LD formation.

In neurons, conditions such as hypoxia, lipid-loading, and neurodegeneration induce formation of LDs (Pennetta and Welte, 2018; Welte et al., 2005). In cultured human cells and primary neurons from mice, α-Syn binds to LDs and increases their accumulation (Cole et al., 2002). Accumulation of α-Syn on LDs reduces hydrolysis of triglycerides contained in the droplets in mammalian cells (Cole et al., 2002). The interactions of α-Syn with LDs may also provide a scaffold for α-Syn aggregation and for the formation of Lewy bodies (Cole et al., 2002; Galvagnion et al., 2015). Consistent with this hypothesis, Lewy bodies contain accumulations of lipid vesicles (Shahmoradian et al., 2019). Alternatively, the process of α-Syn amyloid formation may be in competition with that of membrane binding. Interestingly, LDs have been implicated in several motor neuron diseases and accumulate upon neurodegeneration (Pennetta and Welte, 2018).

Bioinformatic analyses revealed striking similarities between the membrane-targeting motif of α-Syn and that of LD-binding proteins of the perilipin (PLIN) family (Čopič et al., 2018; Giménez-Andrés et al., 2018). PLINs assemble on membranes containing neutral lipids and promote packaging of lipids into membrane-enclosed particles (Bulankina et al., 2009). PLINs are also thought to physically protect LDs from lipase-induced lipolysis (Granneman et al., 2009; Sztalryd and Brasaemle, 2017), and PLINs associate with DAG-rich ER membranes (Skinner et al., 2009). Exogenous expression of mammalian PLINs in yeast results in a phenotype similar to that of α-Syn expression (Jacquier et al., 2013). We propose that α-Syn acts as a PLIN to trigger the formation of LDs or to stabilize them once they are formed by protecting them from the action of

(B) Observed biomass of strains expressing α-Syn and a Pah1 mutant (biomass[α-Syn + *pah1* mutant]) was compared to expected biomass based on each perturbation alone (biomass[α-Syn]*biomass[*pah1* mutant]). Biomass data from (A) were used (two-way ANOVA adjusted for multiple comparisons, alpha = 0.05).
(C) Schematic depicting possible downstream effects of phosphorylated Pah1 with inhibitors highlighted in red.
(D and E) Normalized biomass of indicated yeast strains measured in the presence or absence of (D) 75 μM inositol (n = 3) or (E) 2 mM propranolol ($n \geq 3$; one-way ANOVA adjusted for multiple comparisons, alpha = 0.05).
(F) Viability of mouse N2A cells treated with α-Syn fibrils preformed from recombinant protein and then treated for 36 h with vehicle or 10 μM propranolol (two-way ANOVA adjusted for multiple comparisons, n = 4, alpha = 0.05).
(G) Viability of HEK293 cells transfected with a pool of siRNAs designed to inhibit expression of *LPIN1-3* and treated with α-Syn fibrils (unpaired t test, n = 6, alpha = 0.05).
Normalized biomass and cell viability values are displayed as mean ± standard deviation. ****, $p < 0.0001$; ***, $p < 0.001$; **, $p < 0.01$; *, $p < 0.05$.

lipases. A number of previous findings support this hypothesis: Expression of wild-type α-Syn causes accumulation of LDs, whereas expression of mutant A30P α-Syn, which has low affinity for membranes, does not cause LD accumulation in yeast (Outeiro and Lindquist, 2003; Sere et al., 2010) and the A30P mutant does not bind LDs in mammalian cells (Cole et al., 2002). Moreover, removing the N-terminal region of α-Syn responsible for membrane binding abolishes α-Syn toxicity and inclusion formation in yeast (Soper et al., 2008; Vamvaca et al., 2009). In addition, expression of PLINs recovers LD formation in yeast cells with defects in lipid storage caused by deletion of Pah1 (Jacquier et al., 2013), similar to our observation that α-Syn expression is less toxic in *Δpah1* or *pah1*-D398E yeast mutants.

Consistent with our findings, a recent study showed that inhibition of oleic acid biosynthesis in yeast, which is a few biochemical steps upstream of Pah1, rescues cells from α-Syn-induced toxicity. Deletion of *DGA1* and *LRO1*, which encode enzymes that convert DAG to TAG, showed that DAG accumulation enhances toxicity of α-Syn possibly by increasing DAG and oleic acid levels in the ER (Fanning et al., 2019). In contrast, decreased DAG levels resulting from deletion of *TGL3/4* and growth in choline rescue yeast from toxicity (Fanning et al., 2019). Although a role for phospholipid biosynthesis downstream of Pah1 cannot be completely ruled out, our data and data from Fanning et al. suggest that high DAG levels are critical for α-Syn-mediated toxicity. Since yeast cells grow normally when DAG accumulates in the ER [e.g., when *DGK1* is deleted (Adeyo et al., 2011; Fanning et al., 2019; Han et al., 2008)], it is possible that DAG accumulation is only toxic in the presence of α-Syn. We speculate that α-Syn, like PLIN family members (Bulankina et al., 2009; Čopič et al., 2018; Granneman et al., 2009; Jacquier et al., 2013; Skinner et al., 2009), is recruited to membranes with high DAG content altering membrane properties and functions such as trafficking. It remains to be determined if inactivation of Pah1, and the resulting decrease in DAG levels, rescues yeast cells from α-Syn-mediated toxicity primarily because it prevents excessive lipid storage in LDs or because it prevents accumulation of DAG in the ER and subsequent recruitment of α-Syn. Contrasting findings have been reported regarding the toxicity of α-Syn in yeast that cannot form LDs (Fanning et al., 2019; Sere et al., 2010), and the localization of α-Syn in the absence of LDs in yeast remains to be shown.

Data from mammalian models of α-Syn toxicity and human cohorts suggest that some of the mechanisms that drive toxicity of α-Syn in yeast are conserved in higher organisms and may be relevant to PD. Our mammalian cell toxicity model is based on internalization of pre-formed α-Syn amyloid fibrils, whereas our yeast model is based on α-Syn expression. Therefore, the intracellular conformational states of α-Syn may differ in the two models. Despite this, inhibition of LPIN1/2/3 with propranolol in neuronal cells and silencing of *LPIN* genes in human cells treated with α-Syn fibrils both reduced α-Syn toxicity. Consistent with these results, silencing of all *LPIN* genes reduced α-Syn toxicity in rat cortical neurons, and DAG accumulation was detected in a PD mouse model and in neurons with an α-Syn triplication (Fanning et al., 2019). In support of our proposed mechanism and its relevance to PD, the gene coding for DGKQ, which catalyzes the conversion of DAG to PA, the reverse of the reaction catalyzed by Pah1 and LPINs, is associated with an increased risk for PD (Nalls et al., 2014).

A recent study showed that B2AR is a regulator of α-Syn expression through histone acetylation of its promoter and enhancers and that agonists of B2AR are protective in Parkinson disease models (Mittal et al., 2017). In this same study, propranolol, an FDA-approved beta-adrenergic receptor antagonist, was shown to increase α-Syn expression and to be associated with an increased risk of PD. Here we demonstrated that propranolol suppressed toxicity due to α-Syn expression in yeast and α-Syn fibril-treated neuroblastoma cells. Yeast cells used in our screen lack B2AR and α-Syn was not expressed from the endogenous promoter; therefore, in our model the protective effects of propranolol prevailed. Similarly, N2A cells, the neuronal model we used, do not express detectable levels of B2AR (Hornburg et al., 2014), and toxicity was induced by exogenous pre-formed fibrils. This could explain why the protective effects of propranolol were not previously observed, but additional work will be necessary to definitively explain these findings. Given the increased risk of PD associated with propranolol use and the potential off-target effects of the drug, we do not support its testing as a PD therapy; however, more selective LPIN or CTDNEP1 (the latter is the human ortholog of yeast *NEM1*) inhibitors may hold promise for treatment of PD.

Our rapid and information-rich sentinel screening approach simultaneously measures several hundred validated biological markers, each representative of activation of the corresponding pathway or module. This screen can be tailored to include perturbation-specific markers as we did here for α-Syn. Although we focused here on Pah1, our screen predicted that modulation of other pathways leads to rescue from α-Syn-induced toxicity. One of these pathways involves Ero1, a marker for ER protein folding, a process previously implicated in α-Syn toxicity in yeast and in MPP^+ Parkinson models (Lehtonen et al., 2016). Simultaneous perturbation of multiple pathways identified in our screen may also lead to stronger rescue effects. Based on our partial regression plots, alterations of the phosphorylation status of Osh1 and Num1 are promising targets to combine with deactivation of Pah1. Intriguingly, the oxysterol-binding proteins Osh2 and Osh3 were previously discovered as genetic modulators of α-Syn toxicity (Yeger-Lotem et al., 2009). Num1, a protein involved in the mitochondria-ER-cortex-anchor (Lackner et al., 2013), may provide another link between α-Syn and Pah1 at the ER. We suggest testing of these candidates in future studies aimed at assessing combinatorial effects on rescue.

The network analysis of paths linking genetic modulators to Pah1 suggests mechanistic hypotheses regarding the roles of previously reported toxicity modifiers. For example, altering vesicle trafficking, and its modulators, may influence Pah1 through Nup84, a genetic interactor of the Nem1-Spo7 complex (Siniossoglou et al., 1998). Similarly, the path from Ykt6 through the Sec1-Sso1-Sso2-Sec22 network to Pkc1 may link autophagy to Pah1 and α-Syn rescue and may explain previous reports that these processes moderate α-Syn toxicity (Bas et al., 2018; Nair et al., 2011; Reggiori and Klionsky, 2013; Sakaki et al., 2008). Thus, the Pah1 network analysis provides context for the top candidate from our screen and is a source of testable hypotheses on interventions that could decrease α-Syn-induced

toxicity. In summary, relating pathway activation data to quantitative growth assays, as we did here through linear regression analyses, allows connection of modulators to their effectors and enables formulation of testable mechanistic hypotheses. Acquiring network fingerprints across a variety of conditions may also provide ideal perturbative datasets for network reconstruction or reverse engineering and for uncovering regulatory links among pathways.

STAR★METHODS

Detailed methods are provided in the online version of this paper and include the following:

- KEY RESOURCES TABLE
- LEAD CONTACT AND MATERIALS AVAILABILITY
- EXPERIMENTAL MODEL AND SUBJECT DETAILS
  - Saccharomyces cerevisiae
  - Mammalian Cell Lines
- METHOD DETAILS
  - Yeast Strain Phenotyping
  - Shotgun Proteomic Analysis
  - Quantification of Modulator Rescue
  - Addition of α-Syn-Specific Markers to the Sentinel Assay
  - Pathway Monitoring across α-Syn Modulators
  - Data Processing and Modeling of Rescue
  - Enrichment Analysis of Sentinels Oppositely Regulated between Enhancers and Suppressors
  - Network Analysis of α-Syn Genetic Modulators and Pah1 Regulators
  - Strain Construction and Growth Assessment
  - Live-Cell Microscopy
  - Quantification of α-Syn Abundance
  - Quantification of Pah1 Phosphorylation
  - Pah1 Perturbation and Rescue Assessment
  - Analysis of Interactions between α-Syn Expression and *PAH1* Mutants
  - Suppression of Toxicity by Propranolol in Mammalian Neuroblast Cells
  - Suppression of Toxicity by Knockdown of Lipin Genes in Human Cells
- QUANTIFICATION AND STATISTICAL ANALYSIS
- DATA AND CODE AVAILABILITY

SUPPLEMENTAL INFORMATION

Supplemental Information can be found online at https://doi.org/10.1016/j.cels.2019.07.010.

ACKNOWLEDGMENTS

We are grateful to George Carman and Gil Soo-Han (Rutgers University) for sharing plasmids of *PAH1* mutants and to Susan Lindquist, Pavan Auluck, Saranna Fanning, and Gabriela Caraveo (Whitehead Institute for Biomedical Research) for sharing α-Syn strains and for insightful discussions. We thank Sung Sik Lee and Samuel Gilberto (ETH Zurich) for advice on microscopy analyses. We thank Roger Schneiter (University of Fribourg) for useful advice. This project was supported by a European Research Council (ERC) Starting grant (no. 337965), a Swiss National Science Foundation Professorship (no. PP00P3_133670/1), Sinergia grants CRSII3_154461 and 177195, a Personalized Health and Related Technologies Grant (PHRT-506), and funding from the Neuroscience Center Zurich (ZNZ) and the Gelu Foundation. S.V. acknowledges support from the Swiss National Science Foundation grant #163966. A.B. and K.C. are supported by the German Federal Ministry of Education and Research Grants Sybacol and PhosphoNetPPM.

AUTHOR CONTRIBUTIONS

M.S., F.L., J.A.G., M.vO., L.M., P.J.B., and N.C.P. performed experiments and analyzed data. K.C. performed the regression and network analyses. P.J.B. contributed to development of mass spectrometry methods. R.R. and M.P. provided tools. S.V. analyzed data and contributed to the final model. M.S., K.C., S.V., A.B., and P.P. wrote the manuscript with input from other authors. A.B. and P.P. conceived and supervised the project.

DECLARATION OF INTERESTS

The authors declare no competing interests.

Received: October 23, 2018
Revised: April 17, 2019
Accepted: July 23, 2019
Published: September 11, 2019

REFERENCES

Adeyo, O., Horn, P.J., Lee, S.K., Binns, D.D., Chandrahas, A., Chapman, K.D., and Goodman, J.M. (2011). The yeast lipin orthologue Pah1p is important for biogenesis of lipid droplets. J. Cell Biol. *192*, 1043–1055.

Ashburner, M., Ball, C.A., Blake, J.A., Botstein, D., Butler, H., Cherry, J.M., Davis, A.P., Dolinski, K., Dwight, S.S., Eppig, J.T., et al. (2000). Gene ontology: tool for the unification of biology. The Gene Ontology Consortium. Nat. Genet. *25*, 25–29.

Barbosa, A.D., Sembongi, H., Su, W.M., Abreu, S., Reggiori, F., Carman, G.M., and Siniossoglou, S. (2015). Lipid partitioning at the nuclear envelope controls membrane biogenesis. Mol. Biol. Cell *26*, 3641–3657.

Bas, L., Papinski, D., Licheva, M., Torggler, R., Rohringer, S., Schuschnig, M., and Kraft, C. (2018). Reconstitution reveals Ykt6 as the autophagosomal SNARE in autophagosome-vacuole fusion. J. Cell Biol. *217*, 3656–3669.

Briatte, F. (2016). Ggnetwork: geometries to Plot Networks with "ggplot2".

Bulankina, A.V., Deggerich, A., Wenzel, D., Mutenda, K., Wittmann, J.G., Rudolph, M.G., Burger, K.N.J., and Höning, S. (2009). TIP47 functions in the biogenesis of lipid droplets. J. Cell Biol. *185*, 641–655.

Butts, C.T. (2008). Network: a package for managing relational data in R. J. Stat. Software *1*.

Cherkasova, V.A. (2006). Measuring MAP kinase activity in immune complex assays. Methods *40*, 234–242.

Cherry, J.M., Hong, E.L., Amundsen, C., Balakrishnan, R., Binkley, G., Chan, E.T., Christie, K.R., Costanzo, M.C., Dwight, S.S., Engel, S.R., et al. (2012). Saccharomyces Genome Database: the genomics resource of budding yeast. Nucleic Acids Res. *40*, D700–D705.

Choi, H.S., Su, W.M., Morgan, J.M., Han, G.S., Xu, Z., Karanasios, E., Siniossoglou, S., and Carman, G.M. (2011). Phosphorylation of phosphatidate phosphatase regulates its membrane association and physiological functions in Saccharomyces cerevisiae: identification of SER(602), THR(723), and SER(744) as the sites phosphorylated by CDC28 (CDK1)-encoded cyclin-dependent kinase. J. Biol. Chem. *286*, 1486–1498.

Choi, M., Chang, C.Y., Clough, T., Broudy, D., Killeen, T., MacLean, B., and Vitek, O. (2014). MSstats: an R package for statistical analysis of quantitative mass spectrometry-based proteomic experiments. Bioinformatics *30*, 2524–2526.

Chung, C.Y., Khurana, V., Auluck, P.K., Tardiff, D.F., Mazzulli, J.R., Soldner, F., Baru, V., Lou, Y., Freyzon, Y., Cho, S., et al. (2013). Identification and rescue of α-synuclein toxicity in Parkinson patient-derived neurons. Science *342*, 983–987.

Cole, N.B., Murphy, D.D., Grider, T., Rueter, S., Brasaemle, D., and Nussbaum, R.L. (2002). Lipid droplet binding and oligomerization properties of the Parkinson's disease protein alpha-synuclein. J. Biol. Chem. *277*, 6344–6352.

Cooper, A.A., Gitler, A.D., Cashikar, A., Haynes, C.M., Hill, K.J., Bhullar, B., Liu, K., Xu, K., Strathearn, K.E., Liu, F., et al. (2006). Alpha-synuclein blocks ER-Golgi traffic and rab1 rescues neuron loss in Parkinson's models. Science *313*, 324–328.

Čopič, A., Antoine-Bally, S., Giménez-Andrés, M., La Torre Garay, C., Antonny, B., Manni, M.M., Pagnotta, S., Guihot, J., and Jackson, C.L. (2018). A giant amphipathic helix from a perilipin that is adapted for coating lipid droplets. Nat. Commun. *9*, 1332.

Csardi, G., and Nepusz, T. (2006). The igraph software package for complex network research. InterJournal Complex Systems, 1695.

Fanning, S., Haque, A., Imberdis, T., Baru, V., Barrasa, M.I., Nuber, S., Termine, D., Ramalingam, N., Ho, G.P.H., Noble, T., et al. (2019). Lipidomic analysis of α-synuclein neurotoxicity identifies stearoyl CoA desaturase as a target for Parkinson treatment. Mol. Cell *73*, 1001–1014.e8.

Fares, M.B., Maco, B., Oueslati, A., Rockenstein, E., Ninkina, N., Buchman, V.L., Masliah, E., and Lashuel, H.A. (2016). Induction of de novo α-synuclein fibrillization in a neuronal model for Parkinson's disease. Proc. Natl. Acad. Sci. USA *113*, E912–E921.

Galvagnion, C., Buell, A.K., Meisl, G., Michaels, T.C.T., Vendruscolo, M., Knowles, T.P.J., and Dobson, C.M. (2015). Lipid vesicles trigger α-synuclein aggregation by stimulating primary nucleation. Nat. Chem. Biol. *11*, 229–234.

Gerez, J.A., Prymaczok, N.C., Rockenstein, E., Herrmann, U.S., Schwarz, P., Adame, A., Enchev, R.I., Courtheoux, T., Boersema, P.J., Riek, R., et al. (2019). A cullin-RING ubiquitin ligase targets exogenous α-synuclein and inhibits Lewy body-like pathology. Sci. Transl. Med. *11*, eaau6722.

Giménez-Andrés, M., Čopič, A., and Antonny, B. (2018). The many faces of amphipathic helices. Biomolecules *8*, 45.

Gitler, A.D., Chesi, A., Geddie, M.L., Strathearn, K.E., Hamamichi, S., Hill, K.J., Caldwell, K.A., Caldwell, G.A., Cooper, A.A., Rochet, J.C., et al. (2009). Alpha-synuclein is part of a diverse and highly conserved interaction network that includes PARK9 and manganese toxicity. Nat. Genet. *41*, 308–315.

Glatter, T., Ludwig, C., Ahrné, E., Aebersold, R., Heck, A.J.R., and Schmidt, A. (2012). Large-scale quantitative assessment of different in-solution protein digestion protocols reveals superior cleavage efficiency of tandem Lys-C/trypsin proteolysis over trypsin digestion. J. Proteome Res. *11*, 5145–5156.

Granneman, J.G., Moore, H.P., Krishnamoorthy, R., and Rathod, M. (2009). Perilipin controls lipolysis by regulating the interactions of AB-hydrolase containing 5 (Abhd5) and adipose triglyceride lipase (Atgl). J. Biol. Chem. *284*, 34538–34544.

Han, G.S., O'Hara, L., Siniossoglou, S., and Carman, G.M. (2008). Characterization of the yeast DGK1-encoded CTP-dependent diacylglycerol kinase. J. Biol. Chem. *283*, 20443–20453.

Han, G.S., Siniossoglou, S., and Carman, G.M. (2007). The cellular functions of the yeast lipin homolog PAH1p are dependent on its phosphatidate phosphatase activity. J. Biol. Chem. *282*, 37026–37035.

Henry, S.A., Kohlwein, S.D., and Carman, G.M. (2012). Metabolism and regulation of glycerolipids in the yeast Saccharomyces cerevisiae. Genetics *190*, 317–349.

Hornburg, D., Drepper, C., Butter, F., Meissner, F., Sendtner, M., and Mann, M. (2014). Deep proteomic evaluation of primary and cell line motoneuron disease models delineates major differences in neuronal characteristics. Mol. Cell. Proteomics *13*, 3410–3420.

Hsieh, L.S., Su, W.M., Han, G.S., and Carman, G.M. (2015). Phosphorylation regulates the ubiquitin-independent degradation of yeast Pah1 phosphatidate phosphatase by the 20S proteasome. J. Biol. Chem. *290*, 11467–11478.

Hsieh, L.S., Su, W.M., Han, G.S., and Carman, G.M. (2016). Phosphorylation of yeast Pah1 phosphatidate phosphatase by casein kinase II regulates its function in lipid metabolism. J. Biol. Chem. *291*, 9974–9990.

Jacquier, N., Mishra, S., Choudhary, V., and Schneiter, R. (2013). Expression of oleosin and perilipins in yeast promotes formation of lipid droplets from the endoplasmic reticulum. J. Cell Sci. *126*, 5198–5209.

Khurana, V., and Lindquist, S. (2010). Modelling neurodegeneration in Saccharomyces cerevisiae: why cook with Baker's yeast? Nat. Rev. Neurosci. *11*, 436–449.

Khurana, V., Peng, J., Chung, C.Y., Auluck, P.K., Fanning, S., Tardiff, D.F., Bartels, T., Koeva, M., Eichhorn, S.W., Benyamini, H., et al. (2017). Genome-scale networks link neurodegenerative disease genes to α-synuclein through specific molecular pathways. Cell Syst. *4*, 157–170.

Klionsky, D.J. (2007). Autophagy: from phenomenology to molecular understanding in less than a decade. Nat. Rev. Mol. Cell Biol. *8*, 931–937.

Lackner, L.L., Ping, H., Graef, M., Murley, A., and Nunnari, J. (2013). Endoplasmic reticulum-associated mitochondria-cortex tether functions in the distribution and inheritance of mitochondria. Proc. Natl. Acad. Sci. USA *110*, E458–E467.

Lehtonen, Š., Jaronen, M., Vehviläinen, P., Lakso, M., Rudgalvyte, M., Keksa-Goldsteine, V., Wong, G., Courtney, M.J., Koistinaho, J., and Goldsteins, G. (2016). Inhibition of excessive oxidative protein folding is protective in MPP(+) toxicity-induced Parkinson's disease models. Antioxid. Redox Signal *25*, 485–497.

Longtine, M.S., McKenzie, A., Demarini, D.J., Shah, N.G., Wach, A., Brachat, A., Philippsen, P., and Pringle, J.R. (1998). Additional modules for versatile and economical PCR-based gene deletion and modification in Saccharomyces cerevisiae. Yeast *14*, 953–961.

Luk, K.C., Kehm, V., Carroll, J., Zhang, B., O'Brien, P., Trojanowski, J.Q., and Lee, V.M.-Y. (2012). Pathological α-synuclein transmission initiates Parkinson-like neurodegeneration in nontransgenic mice. Science *338*, 949–953.

Luk, K.C., Song, C., O'Brien, P., Stieber, A., Branch, J.R., Brunden, K.R., Trojanowski, J.Q., and Lee, V.M.-Y. (2009). Exogenous alpha-synuclein fibrils seed the formation of Lewy body-like intracellular inclusions in cultured cells. Proc. Natl. Acad. Sci. USA *106*, 20051–20056.

Makanae, K., Kintaka, R., Makino, T., Kitano, H., and Moriya, H. (2013). Identification of dosage-sensitive genes in Saccharomyces cerevisiae using the genetic tug-of-war method. Genome Res. *23*, 300–311.

Mani, R., St Onge, R.P., Hartman, J.L., Giaever, G., and Roth, F.P. (2008). Defining genetic interaction. Proc. Natl. Acad. Sci. USA *105*, 3461–3466.

Meinshausen, N., and Bühlmann, P. (2010). Stability selection. J. R. Stat. Soc. *72*, 417–473.

Mewes, H.W., Frishman, D., Güldener, U., Mannhaupt, G., Mayer, K., Mokrejs, M., Morgenstern, B., Münsterkötter, M., Rudd, S., and Weil, B. (2002). MIPS: a database for genomes and protein sequences. Nucleic Acids Res. *30*, 31–34.

Mittal, S., Bjørnevik, K., Im, D.S., Flierl, A., Dong, X., Locascio, J.J., Abo, K.M., Long, E., Jin, M., Xu, B., et al. (2017). B2-adrenoreceptor is a regulator of the α-synuclein gene driving risk of Parkinson's disease. Science *357*, 891–898.

Morlock, K.R., McLaughlin, J.J., Lin, Y.P., and Carman, G.M. (1991). Phosphatidate phosphatase from Saccharomyces cerevisiae. Isolation of 45- and 104-kDa forms of the enzyme that are differentially regulated by inositol. J. Biol. Chem. *266*, 3586–3593.

Nair, U., Jotwani, A., Geng, J., Gammoh, N., Richerson, D., Yen, W.L., Griffith, J., Nag, S., Wang, K., Moss, T., et al. (2011). SNARE proteins are required for macroautophagy. Cell *146*, 290–302.

Nalls, M.A., Pankratz, N., Lill, C.M., Do, C.B., Hernandez, D.G., Saad, M., DeStefano, A.L., Kara, E., Bras, J., Sharma, M., et al. (2014). Large-scale meta-analysis of genome-wide association data identifies six new risk loci for Parkinson's disease. Nat. Genet. *46*, 989–993.

O'Hara, L., Han, G.S., Peak-Chew, S., Grimsey, N., Carman, G.M., and Siniossoglou, S. (2006). Control of phospholipid synthesis by phosphorylation of the yeast lipin Pah1p/Smp2p Mg2+-dependent phosphatidate phosphatase. J. Biol. Chem. *281*, 34537–34548.

Oueslati, A., Fournier, M., and Lashuel, H.A. (2010). Role of post-translational modifications in modulating the structure, function and toxicity of alpha-synuclein: implications for Parkinson's disease pathogenesis and therapies. Prog. Brain Res. *183*, 115–145.

Oueslati, A., Paleologou, K.E., Schneider, B.L., Aebischer, P., and Lashuel, H.A. (2012). Mimicking phosphorylation at serine 87 inhibits the aggregation of human α-synuclein and protects against its toxicity in a rat model of Parkinson's disease. J. Neurosci *32*, 1536–1544.

Outeiro, T.F., and Lindquist, S. (2003). Yeast cells provide insight into alpha-synuclein biology and pathobiology. Science *302*, 1772–1775.

Paleologou, K.E., Schmid, A.W., Rospigliosi, C.C., Kim, H.Y., Lamberto, G.R., Fredenburg, R.A., Lansbury, P.T., Fernandez, C.O., Eliezer, D., Zweckstetter, M., et al. (2008). Phosphorylation at Ser-129 but not the phosphomimics S129E/D inhibits the fibrillation of alpha-synuclein. J. Biol. Chem. *283*, 16895–16905.

Pennetta, G., and Welte, M.A. (2018). Emerging links between lipid droplets and motor neuron diseases. Dev. Cell *45*, 427–432.

Petroi, D., Popova, B., Taheri-Talesh, N., Irniger, S., Shahpasandzadeh, H., Zweckstetter, M., Outeiro, T.F., and Braus, G.H. (2012). Aggregate clearance of α-synuclein in Saccharomyces cerevisiae depends more on autophagosome and vacuole function than on the proteasome. J. Biol. Chem. *287*, 27567–27579.

Polymeropoulos, M.H., Lavedan, C., Leroy, E., Ide, S.E., Dehejia, A., Dutra, A., Pike, B., Root, H., Rubenstein, J., Boyer, R., et al. (1997). Mutation in the alpha-synuclein gene identified in families with Parkinson's disease. Science *276*, 2045–2047.

Ramirez, A., Heimbach, A., Gründemann, J., Stiller, B., Hampshire, D., Cid, L.P., Goebel, I., Mubaidin, A.F., Wriekat, A.L., Roeper, J., et al. (2006). Hereditary parkinsonism with dementia is caused by mutations in ATP13A2, encoding a lysosomal type 5 P-type ATPase. Nat. Genet. *38*, 1184–1191.

Reggiori, F., and Klionsky, D.J. (2013). Autophagic processes in yeast: mechanism, machinery and regulation. Genetics *194*, 341–361.

Robinson, M.D., Grigull, J., Mohammad, N., and Hughes, T.R. (2002). FunSpec: a web-based cluster interpreter for yeast. BMC Bioinformatics *3*, 35.

Sakaki, K., Wu, J., and Kaufman, R.J. (2008). Protein kinase C theta is required for autophagy in response to stress in the endoplasmic reticulum. J. Biol. Chem. *283*, 15370–15380.

Santos-Rosa, H., Leung, J., Grimsey, N., Peak-Chew, S., and Siniossoglou, S. (2005). The yeast lipin Smp2 couples phospholipid biosynthesis to nuclear membrane growth. EMBO J *24*, 1931–1941.

Sasser, T., Qiu, Q.S., Karunakaran, S., Padolina, M., Reyes, A., Flood, B., Smith, S., Gonzales, C., and Fratti, R.A. (2012). Yeast lipin 1 orthologue pah1p regulates vacuole homeostasis and membrane fusion. J. Biol. Chem. *287*, 2221–2236.

Sere, Y.Y., Regnacq, M., Colas, J., and Berges, T. (2010). A Saccharomyces cerevisiae strain unable to store neutral lipids is tolerant to oxidative stress induced by α-synuclein. Free Radic. Biol. Med *49*, 1755–1764.

Shahmoradian, S.H., Lewis, A.J., Genoud, C., Hench, J., Moors, T.E., Navarro, P.P., Castaño-Díez, D., Schweighauser, G., Graff-Meyer, A., Goldie, K.N., et al. (2019). Lewy pathology in Parkinson's disease consists of crowded organelles and lipid membranes. Nat. Neurosci *22*, 1099–1109.

Sill, M., Hielscher, T., Becker, N., and Zucknick, M. (2014). c060 : extended inference with lasso and elastic-net regularized cox and generalized linear models. J. Stat. Soft *62*, 1–22.

Singleton, A.B., Farrer, M., Johnson, J., Singleton, A., Hague, S., Kachergus, J., Hulihan, M., Peuralinna, T., Dutra, A., Nussbaum, R., et al. (2003). Alpha-synuclein locus triplication causes Parkinson's disease. Science *302*, 841.

Siniossoglou, S., Santos-Rosa, H., Rappsilber, J., Mann, M., and Hurt, E. (1998). A novel complex of membrane proteins required for formation of a spherical nucleus. EMBO J *17*, 6449–6464.

Skinner, J.R., Shew, T.M., Schwartz, D.M., Tzekov, A., Lepus, C.M., Abumrad, N.A., and Wolins, N.E. (2009). Diacylglycerol enrichment of endoplasmic reticulum or lipid droplets recruits perilipin 3/TIP47 during lipid storage and mobilization. J. Biol. Chem. *284*, 30941–30948.

Snead, D., and Eliezer, D. (2014). Alpha-synuclein function and dysfunction on cellular membranes. Exp. Neurobiol. *23*, 292–313.

Soper, J.H., Roy, S., Stieber, A., Lee, E., Wilson, R.B., Trojanowski, J.Q., Burd, C.G., and Lee, V.M.-Y. (2008). α-synuclein–induced Aggregation of Cytoplasmic Vesicles in *Saccharomyces cerevisiae*. Mol. Biol. Cell *19*, 1093–1103.

Soste, M., Hrabakova, R., Wanka, S., Melnik, A., Boersema, P., Maiolica, A., Wernas, T., Tognetti, M., Von Mering, C., and Picotti, P. (2014). A sentinel protein assay for simultaneously quantifying cellular processes. Nat. Methods *11*, 1045–1048.

Spillantini, M.G., Schmidt, M.L., Lee, V.M.-Y., Trojanowski, J.Q., Jakes, R., and Goedert, M. (1997). Alpha-synuclein in Lewy bodies. Nature *388*, 839–840.

Su, W.M., Han, G.S., and Carman, G.M. (2014). Yeast Nem1-Spo7 protein phosphatase activity on Pah1 phosphatidate phosphatase is specific for the Pho85-Pho80 protein kinase phosphorylation sites. J. Biol. Chem. *289*, 34699–34708.

Su, W.M., Han, G.S., Casciano, J., and Carman, G.M. (2012). Protein kinase A-mediated phosphorylation of Pah1p phosphatidate phosphatase functions in conjunction with the Pho85p-Pho80p and Cdc28p-cyclin B kinases to regulate lipid synthesis in yeast. J. Biol. Chem. *287*, 33364–33376.

Suzuki, K., Kamada, Y., and Ohsumi, Y. (2002). Studies of cargo delivery to the vacuole mediated by autophagosomes in Saccharomyces cerevisiae. Dev. Cell *3*, 815–824.

Szklarczyk, D., Gable, A.L., Lyon, D., Junge, A., Wyder, S., Huerta-Cepas, J., Simonovic, M., Doncheva, N.T., Morris, J.H., Bork, P., et al. (2019). STRING v11: protein-protein association networks with increased coverage, supporting functional discovery in genome-wide experimental datasets. Nucleic Acids Res. *47*, D607–D613.

Sztalryd, C., and Brasaemle, D.L. (2017). The perilipin family of lipid droplet proteins: gatekeepers of intracellular lipolysis. Biochim. Biophys. Acta Mol. Cell Biol. Lipids *1862*, 1221–1232.

Tardiff, D.F., Jui, N.T., Khurana, V., Tambe, M.A., Thompson, M.L., Chung, C.Y., Kamadurai, H.B., Kim, H.T., Lancaster, A.K., Caldwell, K.A., et al. (2013). Yeast reveal a "druggable" Rsp5/Nedd4 network that ameliorates α-synuclein toxicity in neurons. Science *342*, 979–983.

Theillet, F.X., Binolfi, A., Bekei, B., Martorana, A., Rose, H.M., Stuiver, M., Verzini, S., Lorenz, D., van Rossum, M., Goldfarb, D., et al. (2016). Structural disorder of monomeric α-synuclein persists in mammalian cells. Nature *530*, 45–50.

Vamvaca, K., Volles, M.J., and Lansbury, P.T. (2009). The first N-terminal amino acids of alpha-synuclein are essential for alpha-helical structure formation in vitro and membrane binding in yeast. J. Mol. Biol. *389*, 413–424.

Wang, S., Horn, P.J., Liou, L.C., Muggeridge, M.I., Zhang, Z., Chapman, K.D., and Witt, S.N. (2013). A peroxisome biogenesis deficiency prevents the binding of alpha-synuclein to lipid droplets in lipid-loaded yeast. Biochem. Biophys. Res. Commun. *438*, 452–456.

Welte, M.A., Cermelli, S., Griner, J., Viera, A., Guo, Y., Kim, D.H., Gindhart, J.G., and Gross, S.P. (2005). Regulation of lipid-droplet transport by the perilipin homolog LSD2. Curr. Biol. *15*, 1266–1275.

White, M.J., Hirsch, J.P., and Henry, S.A. (1991). The OPI1 gene of Saccharomyces cerevisiae, a negative regulator of phospholipid biosynthesis, encodes a protein containing polyglutamine tracts and a leucine zipper. J. Biol. Chem. *266*, 863–872.

Willingham, S., Outeiro, T.F., DeVit, M.J., Lindquist, S.L., and Muchowski, P.J. (2003). Yeast genes that enhance the toxicity of a mutant huntingtin fragment or alpha-synuclein. Science *302*, 1769–1772.

Yeger-Lotem, E., Riva, L., Su, L.J., Gitler, A.D., Cashikar, A.G., King, O.D., Auluck, P.K., Geddie, M.L., Valastyan, J.S., Karger, D.R., et al. (2009). Bridging high-throughput genetic and transcriptional data reveals cellular responses to alpha-synuclein toxicity. Nat. Genet. *41*, 316–323.

STAR★METHODS

KEY RESOURCES TABLE

REAGENT or RESOURCE	SOURCE	IDENTIFIER
Antibodies		
Anti-Alpha-synuclein, mouse monoclonal [LB 509]	Abcam	Cat#ab27766; RRID:AB_727020
Bacterial Strains		
E.coli: 10-beta Competent *E. coli* (High Efficiency)	New England Biolabs	Cat#C3019I
Chemicals, Peptides, and Recombinant Proteins		
TCEP (tris(2-carboxyethyl)phosphine hydrochloride)	Pierce	Cat#20490; CAS#51805-45-9
Iodoacetamide	Sigma-Aldrich	Cat#I1149 ; CAS#144-48-9
Ammonium bicarbonate	Sigma-Aldrich	Cat#09830; CAS#1066-33-7
Urea	Sigma-Aldrich	Cat#U5128; CAS#57-13-6
Formic acid 98-100%	AppliChem	Cat#A38580500
Acetonitrile (HPLC)	Fisher Chemical	Cat#A998; CAS#75-05-8
Trifluoroacetic acid (HPLC)	Sigma-Aldrich	Cat#302031; CAS#76-05-1
Lysyl endopeptidase	Wako Pure Chemical Industries	Cat#125-05061
Trypsin: sequencing-grade modified trypsin	Promega	Cat#V5111
Titansphere Phos-TiO beads	GL Sciences	Cat#GL-5010-21315
Reprosil-Pur 120 C18-AQ, 3 μm 15 % C endc.	Dr. Maisch GmbH	Cat#r13.aq
Reprosil-Pur 120 C18-AQ, 1.9 μm 15 % C endc.	Dr. Maisch GmbH	Cat#r119.aq
β-Estradiol	Sigma-Aldrich	Cat#E8875; CAS#50-28-2
G418	Matthias Peter Lab	CAS#108321-42-2
NotI-HF	New England BioLabs	Cat#R3189S
XmaI	New England BioLabs	Cat#R0180S
Propranolol hydrochloride	Sigma-Aldrich	Cat#P0884; CAS#318-98-9
myo-Inositol	Karsten Weis Lab	CAS#87-89-8
Nile Red	Thermo Fisher Scientific	Cat#N1142; Cas#7385-67-3
Propidium iodide	Sigma-Aldrich	Cat#P4170; CAS#25535-16-4
Recombinant α-Syn	(Gerez et al., 2019)	N/A
SuperScript II reverse transcriptase	Invitrogen	Cat#18064014
RNaseOUT recombinant ribonuclease inhibitor	Invitrogen	Cat#10777019
Random primers	Biodynamics	Cat#B070-40
Critical Commercial Assays		
BCA	Pierce	Cat#23225
CellTiter 96 Non-Radioactive Cell Proliferation Assay (MTT)	Promega	Cat#G4000
iRT Kit	Biognosys AG	Cat#Ki-3002-1
RNeasy Mini Kit	Qiagen	Cat#74104
Deposited Data		
Shotgun Data	PeptideAtlas: PASS01407	http://www.peptideatlas.org/PASS/PASS01407
PRM data	PeptideAtlas: PASS01409	http://www.peptideatlas.org/PASS/PASS01409
Experimental Models: Cell Lines		
Human embryonic kidney 293 (HEK293)	ATCC	CRL-1573
Mouse neuroblastoma (N2A)	ATCC	CCL-131

(*Continued on next page*)

Continued

REAGENT or RESOURCE	SOURCE	IDENTIFIER
Experimental Models: Organisms/Strains		
S. cerevisiae: IntTox/α-Syn: W303 MATa, can1–100, his3-11,15, leu2-3,112, trp1-1, ura3-1, ade2-1, *GAL1*- αSyn-YFP::*HIS3* and *GAL1*-αSyn-YFP::*TRP1*	Pavan Auluck; Susan Lindquist lab; (Cooper et al., 2006)	N/A
S. cerevisiae: Vector/Empty vector: W303 MATa, can1-100, his3-11,15, leu2-3,112, trp1-1, ura3-1, ade2-1, *GAL1*-empty::*HIS3* and *GAL1*-empty::*TRP1*	Pavan Auluck; Susan Lindquist lab; (Cooper et al., 2006)	N/A
S. cerevisiae: GFP: W303 MATa, can1-100, his3-11,15, leu2-3,112, trp1-1, ura3-1, ade2-1, *GAL1*-GFP::*HIS3* and *GAL1*-GFP::*TRP1*	Pavan Auluck; Susan Lindquist lab	N/A
S. cerevisiae: TDP-43-GFP: W303 MATa, can1-100, his3-11,15, leu2-3,112, trp1-1, ura3-1, ade2-1, *GAL1*-TDP-43::*HIS3* and *GAL1*-TDP-43::*TRP1*	Pavan Auluck; Susan Lindquist lab	N/A
S. cerevisiae: FUS: W303 MATα, can1-100, his3-11,15, leu2-3,112, trp1-1, ura3-1, ade2-1, *GAL1*-FUS::*HIS3*	Pavan Auluck; Susan Lindquist lab	N/A
S. cerevisiae: αSyn Δ*nem1*: W303 MATa, can1-100, his3-11,15, leu2-3,112, trp1-1, ura3-1, ade2-1, *GAL1*- αSyn-YFP::*HIS3* and *GAL1*-αSyn-YFP::*TRP1*, *nem1::Kan*	this study	N/A
S. cerevisiae: Vector Δ*nem1*: W303 MATa, can1-100, his3-11,15, leu2-3,112, trp1-1, ura3-1, ade2-1, *GAL1*-empty::*HIS3* and *GAL1*-empty::*TRP1*, *nem1::Kan*	this study	N/A
S. cerevisiae: GFP Δ*nem1*: W303 MATa, can1-100, his3-11,15, leu2-3,112, trp1-1, ura3-1, ade2-1, *GAL1*-GFP::*HIS3* and *GAL1*-GFP::*TRP1*, *nem1::Kan*	this study	N/A
S. cerevisiae: TDP-43-GFP Δ*nem1*: W303 MATa, can1-100, his3-11,15, leu2-3,112, trp1-1, ura3-1, ade2-1, *GAL1*-TDP-43::*HIS3* and *GAL1*-TDP-43::*TRP1*, *nem1::Kan*	this study	N/A
S. cerevisiae: FUS Δ*nem1*: W303 MATα, can1-100, his3-11,15, leu2-3,112, trp1-1, ura3-1, ade2-1, *GAL1*-FUS::*HIS3*, *nem1::Kan*	this study	N/A
S. cerevisiae: αSyn Δ*pah1*: W303 MATa, can1-100, his3-11,15, leu2-3,112, trp1-1, ura3-1, ade2-1, *GAL1*- αSyn-YFP::*HIS3* and *GAL1*-αSyn-YFP::*TRP1*, *pah1::Kan*	this study	N/A
S. cerevisiae: αSyn pah*1*-7A: W303 MATa, can1-100, his3-11,15, leu2-3,112, trp1-1, ura3-1, ade2-1, *GAL1*- αSyn-YFP::*HIS3* and *GAL1*-αSyn-YFP::*TRP1*, *pah1::Kan, pah1-7A::URA3*	this study	N/A
S. cerevisiae: αSyn pah*1*-7D/E: W303 MATa, can1-100, his3-11,15, leu2-3,112, trp1-1, ura3-1, ade2-1, *GAL1*- αSyn-YFP::*HIS3* and *GAL1*-αSyn-YFP::*TRP1*, *pah1::Kan, pah1-7D/E::URA3*	this study	N/A
S. cerevisiae: αSyn *pah1*-D398E: W303 MATa, can1-100, his3-11,15, leu2-3,112, trp1-1, ura3-1, ade2-1, *GAL1*- αSyn-YFP::*HIS3* and *GAL1*-αSyn-YFP::*TRP1*, *pah1::Kan, pah1-D398E::URA3*	this study	N/A
S. cerevisiae: Estradiol-inducible α-Syn: W303 can1-100, his3-11,15, leu2-3,112, trp1-1, ura3-1, ade2-1, α-Syn::*LEU2 and* GAL4-ER-VP16*::TRP1*	Saranna Fanning; Susan Lindquist lab	N/A
S. cerevisiae: Estradiol-inducible α-Syn Δ*pah1*: W303 can1-100, his3-11,15, leu2-3,112, trp1-1, ura3-1, ade2-1, α-Syn::*LEU2 and* GAL4-ER-VP16*::TRP1, pah1::Kan*	this study	N/A

(*Continued on next page*)

Continued

REAGENT or RESOURCE	SOURCE	IDENTIFIER
S. cerevisiae: Estradiol-inducible α-Syn *pah1*-WT: W303 can1-100, his3-11,15, leu2-3,112, trp1-1, ura3-1, ade2-1, α-Syn::*LEU2 and* GAL4-ER-VP16::*TRP1, pah1::Kan, pah1-WT::URA3*	this study	N/A
S. cerevisiae: Estradiol-inducible α-Syn pah*1*-7A: W303 can1-100, his3-11,15, leu2-3,112, trp1-1, ura3-1, ade2-1, α-Syn::*LEU2 and* GAL4-ER-VP16::*TRP1, pah1::Kan, pah1-7A::URA3*	this study	N/A
S. cerevisiae: Estradiol-inducible α-Syn pah*1*-7D/E: W303 can1-100, his3-11,15, leu2-3,112, trp1-1, ura3-1, ade2-1, α-Syn::*LEU2 and* GAL4-ER-VP16::*TRP1, pah1::Kan, pah1-7D/E::URA3*	this study	N/A
S. cerevisiae: Estradiol-inducible α-Syn *pah1*-D398E: W303 can1-100, his3-11,15, leu2-3,112, trp1-1, ura3-1, ade2-1, α-Syn::*LEU2 and* GAL4-ER-VP16::*TRP1, pah1::Kan, pah1-D398E::URA3*	this study	N/A
Oligonucleotides		
See Table S16	this study	N/A
Recombinant DNA		
α-Syn modulator plasmids: each gene in Table S5 in pBY011; CEN, URA3, Amp^R	(Cooper et al., 2006)	N/A
pFA6a-KanMX6	(Longtine et al., 1998)	N/A
pGH315, *pah1* Inserted into pRS415	(Choi et al., 2011)	N/A
pGH315(7A), *pah1* (S110A/S114A/S168A/S602A/T723A/S744A/S748A) inserted into pRS415	(Choi et al., 2011)	N/A
pGH315(7D/E), *pah1* (S110D/S114D/S168D/S602D/T723E/S744D/S748D) inserted into pRS415	(Hsieh et al., 2016)	N/A
pGH312(D398E), HA-tagged *pah1* (D398E)	(Han et al., 2007)	N/A
pRS306, yeast integrative vector with URA3 marker	Matthias Peter Lab	ATCC 77141
pMS1, *pah1*-WT inserted into pRS306	this study	N/A
pMS2, pah*1*-7A inserted into pRS306	this study	N/A
pMS3, *pah1*-D398E inserted into pRS306	this study	N/A
pMS4, pah*1*-7D/E inserted into pRS306	this study	N/A
Software and Algorithms		
Skyline-daily v 2.0.9.4899	Michael MacCoss lab	https://skyline.ms/project/home/software/Skyline/begin.view
R v. 3.1.1 & 3.5.1	The R Project for Statistical Computing	https://www.r-project.org/
MSstats v. 0.99	(Choi et al., 2014)	http://bioconductor.org/packages/release/bioc/html/MSstats.html
Proteome discoverer v. 1.4 & 2.0	Thermo Fisher Scientific	https://www.thermofisher.com/ca/en/home.html
Xcalibur v. 3.1	Thermo Fisher Scientific	https://www.thermofisher.com/ca/en/home.html
Progenesis QI	Nonlinear dynamics	http://www.nonlinear.com/progenesis/qi-for-proteomics/
SafeQuant v. 2.01	(Glatter et al., 2012)	https://cran.r-project.org/web/packages/SafeQuant/index.html
FunSpec	(Robinson et al., 2002)	http://funspec.med.utoronto.ca/
Saccharomyces Genome Database (SGD)	(Cherry et al., 2012)	https://www.yeastgenome.org/
ImageJ v 1.47d	Wayne Rasband, National Institutes of Health, USA	https://imagej.nih.gov/ij/

(*Continued on next page*)

Continued

REAGENT or RESOURCE	SOURCE	IDENTIFIER
CellProfiler v. 3.1.8	CellProfiler cell image analysis software	https://cellprofiler.org/
STRING v. 10.5 & 11.0	(Szklarczyk et al., 2019)	https://string-db.org/
c060 v. 0.2-4	(Sill et al., 2014)	https://cran.r-project.org/web/packages/c060/index.html
igraph v. 1.2.4	(Csardi and Nepusz, 2006)	https://cran.r-project.org/web/packages/igraph/index.html
network v. 1.15	(Butts, 2008)	https://cran.r-project.org/web/packages/network/index.html
ggnetwork v. 0.5.1	(Briatte, 2016)	https://cran.r-project.org/web/packages/ggnetwork/index.html
GraphPad Prism v 7.0c	GraphPad	https://www.graphpad.com/
Other		
FastPrep-24 5G	MP biomedicals	https://ch.mpbio.com/
BioLector	m2p labs	https://www.m2p-labs.com/bioreactors/products/biolector/
FACSCalibur flow cytometer	BD Biosciences	https://www.bd.com/
DM6000B microscope	Leica microsystems	https://www.leica-microsystems.com/
Eclipse Ti microscope	Nikon	https://www.microscope.healthcare.nikon.com
Q-Exactive Plus mass spectrometer	Thermo Fisher Scientific	https://www.thermofisher.com/ca/en/home.html

LEAD CONTACT AND MATERIALS AVAILABILITY

Further information and requests for resources and reagents should be directed to and will be fulfilled by the Lead Contact, Paola Picotti (picotti@imsb.biol.ethz.ch).

EXPERIMENTAL MODEL AND SUBJECT DETAILS

Saccharomyces cerevisiae

Yeast W303 cells were grown at 30°C in synthetic defined (SD) medium picked from a single colony and sampled at 6 h post-induction of α-Syn from log-phase growth, except where specified in Method Details.

Mammalian Cell Lines

Human embryonic kidney 293 (HEK293) cells (sex: female) were grown in Dulbecco's Modified Eagle Media (DMEM) with 10% fetal bovine serum (FBS) and 1% Penicillin-Streptomycin (Pen-Strep) at 37°C and 5% CO_2. Mouse neuroblastoma (N2A) cells (sex: male) were maintained in DMEM with 10% FBS and 1% Pen-Strep, and grown in DMEM with 2% FBS and 1% Pen-Strep when treated with α-Syn pre-formed fibrils. Cell lines were passaged up to 5 times and routinely tested negative for mycoplasma contamination.

METHOD DETAILS

Yeast Strain Phenotyping

Cells were grown overnight at 30 °C in synthetic defined (SD) liquid medium containing 2% glucose with appropriate dropout and then diluted and grown overnight in 2% raffinose dropout medium. To induce α-Syn expression, cells were diluted to 0.3 OD_{600} in 2% galactose SD medium. Live cells were imaged on a Leica DM6000B microscope with a 60X objective in the GFP channel. Images were processed in ImageJ.

For growth assessment, 100 μl of a 0.15 OD_{600} culture in 2% galactose SD medium was transferred to a 96-well plate. Biomass (measured by monitoring 620 nm) was recorded for 24 h by a BioLector microbioreactor. The system was set to a temperature of 30 °C, humidity of 85%, 20.95% O_2, and 800 rpm. The baseline was established on a well-by-well basis according to the average signal of the six time points with the lowest standard deviation across the dataset. Errors are the standard deviations of three biological replicates.

For viability measurements, 100 μl of sample was diluted to 1 ml with PBS and 1 μl of 2 mg/ml propidium iodide was added. Samples were incubated on ice for 10 min in the dark. Cells were pelleted, and the supernatant was discarded. To the sample was added 1 mL of PBS, and 10,000 cells were analyzed by flow cytometry (emission at 617 nm, excitation at 535 nm).

Shotgun Proteomic Analysis

Shotgun proteomic measurements and label-free quantification were carried out on the yeast strain with two copies of α-Syn (IntTox strain) and an empty vector-containing control at 6 h post induction. This time point was selected because α-Syn-YFP inclusions were visible, growth curves of vector- and α-Syn-expressing cells had begun to separate, and death rates were negligible. Cell pellets were mechanically disrupted by bead beating in a FastPrep-24 5G device, protein lysates were digested with trypsin and Lys-C, and peptides were purified and phosphopeptides were isolated using Titansphere Phos-TiO beads as previously described (Soste et al., 2014). Peptides were chromatographically eluted from a 50-cm heated column (60 °C) packed with 1.9-μm C18 beads using a 2-h gradient of 5% to 35% acetonitrile. Peptides were analyzed on a Q-Exactive Plus mass spectrometer operated in DDA mode. Proteins and phosphopeptides were identified by searching the SGD Protein Database with a peptide false discovery rate of < 0.01 using Proteome Discoverer software. MS1 peak identification by Progenesis and quantification and plotting by Safequant (Glatter et al., 2012) were used to find significantly regulated features (fold change ≥ 2, $q \leq 0.01$). Functional enrichment analysis was carried out using FunSpec (Robinson et al., 2002). GO (Ashburner et al., 2000) and MIPS (Mewes et al., 2002) categories were searched. For enriched categories, a significance cutoff of p-value ≤ 0.05 with Bonferroni correction was used.

Quantification of Modulator Rescue

For genetic modulation of toxicity, α-Syn-expressing and empty vector-expressing strains were transformed with an extrachromosomal plasmid for galactose-inducible expression of modulators (Cooper et al., 2006). α-Syn yeast strains expressing the different modulators were cultured in four batches. For the first three batches (13 modulators), cells were grown as described above in three biological replicates. The additional 20 modulators were tested in singlicate as a fourth batch. For induction of α-Syn and modulator expression, cells were diluted to 0.15 OD_{600} in 2% galactose SD medium. Growth was assessed in technical duplicates or triplicates as described above in a microbioreactor. Biomass values were used to quantify rescue. Baselines were established on a well-by-well basis based on averaged signals of the first six time points, then all biomass values over 24 h were summed. The specific rescue by each modulator was calculated by dividing the ratio of the biomass of strain expressing α-Syn plus modulator to strain expressing α-Syn alone by the ratio of the biomass of strain expressing vector plus modulator to vector alone. The mean value of replicates was used for modulators tested in triplicate.

Addition of α-Syn-Specific Markers to the Sentinel Assay

In addition to monitoring generic yeast cellular process (phospho)protein markers (Soste et al., 2014), α-Syn-specific markers were selected from the significantly regulated (phospho)proteins identified in the shotgun proteomic analysis (fold change ≥ 2, $q \leq 0.01$). Proteotypicity was verified, and these targets were measured by PRM targeted mass spectrometry in order to confirm the label-free quantification. Markers were prioritized if the amplitude of their response in PRM and shotgun data was high indicating a greater likelihood for detection in a multiplexed PRM assay and potentially large fold change induced by α-Syn. Phosphopeptide targets were also preferred if their respective protein occurred multiple times in the candidate list, potentially suggesting multiple PTM changes caused by α-Syn. (Phospho)proteins were also prioritized based on their functional characterization and prior knowledge of how this may relate to known α-Syn biology or may lead to novel findings in the case of uncharacterized candidates. Finally, (phospho)proteins with a human homolog were favored to facilitate future testing. Using these criteria, 29 proteins and 65 phosphopeptides were added as α-Syn-specific sentinels. Assays were also generated for S87 phosphorylated α-Syn (added to phosphorylation assay), K12-, K21-, and K96-ubiquitinated α-Syn, the propeptide (YMR297Wpro), and the mature (YMR297Wmat) forms of Cpy1 (all added to protein assay) based on literature evidence of involvement in toxicity. The final proteomic assay attempted to monitor a total of 376 pathway sentinels (188 proteins and 188 phosphopeptides), 26% of which were α-Syn-specific.

Pathway Monitoring across α-Syn Modulators

Quantification of sentinels was done using targeted proteomics as previously described (Soste et al., 2014) except for two differences: the addition of α-Syn-specific sentinels and adaptation of the assay from selected reaction monitoring to PRM mass spectrometry. The assay was implemented on a Q-Exactive Plus mass spectrometer operated in PRM mode. Peptides were eluted from a 20-cm column packed with 3-μm C18 beads using a 5% to 35% acetonitrile gradient over 40 min. iRT peptides were used for scheduling 3-min windows for detecting each target. Raw PRM traces were manually evaluated in Skyline and 3-10 transitions per target and per analysis batch were exported for normalization and quantification by MSStats (Choi et al., 2014). Phosphopeptides and proteins not detected in at least one sample were removed. If a peptide was determined to be detected in all samples but one or more low intensity transitions in some samples had a peak area less than an average noise value (6 transition peak areas where no peptides are detected) then the average noise value, across all batches, was input for the quantification. For protein quantification, noise value was set to a peak area of 2080 and for phosphopeptide quantification, the noise value was set to 3466. In total, 0.0018 of the quantified values were noise values. In total 269/376 sentinels were quantified across 33 genetic modulators in four separate batches. One empty vector, without α-Syn, and one unmodulated α-Syn sample were analyzed in each batch.

Data Processing and Modeling of Rescue

Using the quantified results from MSStats, a phosphopeptide matrix and a protein matrix were created that contained $\log_2$ fold change values relative to the vector sample for 103 phosphosites and 166 proteins across the 37 samples. We corrected for batch effects by subtracting the median value over the batch from the corresponding samples. We chose to use the median as opposed to

the mean for robustness against outliers. Protein and phosphopeptide features were hierarchically clustered in rows according to batch-corrected fold change values relative to the vector samples and using Euclidean distance and the complete linkage method.

We modeled the rescue effect Y as a function of the activities of all sentinels S_j (i.e., the pathway marker abundance values) across all genetic modulators i:

$$Y_i = \alpha + \sum_j \alpha_j S_{ij} + \epsilon_i \quad \text{(Equation 1)}$$

Here, Y_i is the growth effect of modulator i relative to the wild-type control, and S_{ij} is the activity (abundance) of sentinel j for the i^{th} modulator. The fitting parameter α_j is the partial effect of sentinel j on the rescue, and α is the intercept. Since all sentinels are modeled together the effect of the j^{th} sentinel is estimated as if all other sentinels were held constant. The error term in the model is denoted by ϵ_i. In order to retrieve the most relevant sentinels, we aimed to obtain a sparse model using lasso with stability selection (Meinshausen and Bühlmann, 2010). Stability selection is a general approach that combines (regularized) regression models with resampling and aims to find stable sentinels showing strong association with the rescue. Specifically, we used the function 'stabpath' from the R package 'c060' (Sill et al., 2014) with default parameters. The stability selection algorithm was applied twice: once for the phosphopeptides and once for the proteins. We used the average $\log_2$ rescue as a response variable. The input variables were the batch-corrected $\log_2$ fold changes of all 103 phosphopeptides and the batch-corrected $\log_2$ fold changes of all 166 proteins. The protein YMR297W (Cpy1) is a degradation-based sentinel; an increase in propeptide abundance relative to total protein abundance reports the known α-Syn induced block in ER to Golgi vesicle trafficking. The two features YMR297Wpro and YMR297Wmat were therefore counted as one protein sentinel and removed from the protein matrix so that the difference between their values could be considered instead (ratio in the raw space). It was necessary to use regularization since the number of observations/samples (n = 37) is much smaller than the number of variables (p = 103 and 166, respectively). Stable features were classified as sentinels with a maximal selection probability ≥ 0.6. In order to determine the sign of the effect (i.e., coefficient) of the stable features, we fit a linear model, one for the phosphopeptides and one for the proteins, with the same response variable but with the fold changes of the stable features as the sole input variables. As opposed to simple linear regression/correlation analysis, in multiple linear regression the coefficient of each feature measures the effect of that feature on the output given that the values for all other features in the model are held constant. Equivalently, it measures the unique effect of that feature on the output by removing the linear effects of all other features. When two sentinels are correlated to each other (positively or negatively) the coefficients in the combined model may deviate substantially from simple pairwise correlations between sentinels and responses.

Enrichment Analysis of Sentinels Oppositely Regulated between Enhancers and Suppressors

A cluster of 107 sentinels was observed to be oppositely regulated when comparing genetic enhancers and suppressors of toxicity. These sentinels mapped to 100 unique yeast proteins. Funspec was used to test for functional classes enriched in this set of proteins. Using Bonferroni correction and a p-value cutoff of 0.05, GO and MIPS categories were identified.

Network Analysis of α-Syn Genetic Modulators and Pah1 Regulators

The STRING network for *Saccharomyces cerevisiae* was filtered for high-confidence edges (interaction score above 0.9), and subsequently the largest connected component was retained. This consisted of 4,084 nodes and 54,540 edges. The *Saccharomyces* genome database was used to link systematic names (STRING identifiers) and standard names (Cherry et al., 2012). Of the 33 genetic modulators, 25 were present in the largest component. Pah1 was also present in this component. For each of the 25 modulators present in the largest connected component we computed all shortest paths to each of the following upstream regulators of Pah1: Nem1-Spo7 complex components (Nem1, Spo7), Cdc28, PKA complex components (Bcy1, Tpk1/2/3), casein kinase II complex components (Cka1/2, Ckb1/2), Pho80-85 complex (Pho80, Pho85), and Pkc1. This procedure identified the shortest path (or paths) from each modulator to all 14 regulators of Pah1 phosphorylation. We kept the shortest (of the shortest to all regulators) in order to identify the closest of the 14 Pah1 regulator(s). Ties can arise at two stages: if more than one regulator is equally close to a given genetic modulator and if there are multiple shortest paths leading to the same closest regulator. In the case of ties, we kept all shortest paths for the subsequent analysis. The nodes included in the shortest (of the shortest) paths, together with Nem1, Pho80, and Pho85 (i.e., protein Pah1 regulators that are not the closest target of any of the 25 modulators), were used to finally generate the subnetwork. The closest regulator was annotated for each modulator. Eight modulators not found in the largest component were kept as isolated nodes. Since the STRING network is undirected, we excluded Pah1 from the largest connected component when computing the shortest paths because we assumed that Pah1 is the downstream endpoint of the regulators (i.e., to avoid artifacts, the discovered shortest path was not permitted to go from a modulator through Pah1 to one of the regulators).

In order to annotate the correspondence between Pah1 phosphorylation fold change (FC) induced by a given modulator and the network path distance of the same modulator to the closest Pah1 regulator, the absolute FC value was plotted against the length of the shortest distance path. Infinite (Inf) indicates that the modulator was not connected to any Pah1 regulator in the network. To test if modulators closer to Pah1 regulators had a greater average absolute FC, a one-tailed (two-sample) t-test was applied to the group of modulators at shortest distance equal to 1 or 2 compared to those at 3, 4 or Inf.

In order to identify central nodes, we computed for each node of the subgraph its betweenness (i.e., the number of shortest paths going through that node). More specifically, the betweenness centrality of a node v is given by the expression:

$$g(v) = \sum_{s \neq v \neq t} \frac{\sigma_{st}(v)}{\sigma_{st}} \quad \text{(Equation 2)}$$

where σ_{st} is the total number of shortest paths from node s to node t and $\sigma_{st}(v)$ is the number of those paths that pass through v. This score was chosen as a measure of centrality because we previously computed the shortest paths in order to generate the subnetwork.

Strain Construction and Growth Assessment

Deletions of *NEM1* and *PAH1* were done using standard procedures by targeting the KanMX cassette to each target gene (Longtine et al., 1998). Colonies selected by growth in G418 were confirmed to have the correct gene deletion by PCR and sequencing. *pah1*-WT, *pah1–7A*, *pah1–7D/E*, and *pah1*-D398E genes were amplified from plasmids that were a generous gift from George Carman and Gil-Soo Han (Rutgers University) (Choi et al., 2011) and were integrated at the *URA* locus via the vector pRS306. Yeast transformations were done using standard procedures. Serial dilutions of 0.3 OD raffinose cultures of yeast strains were spotted onto glucose and galactose plates and imaged 3 days after spotting in biological triplicate.

Live-Cell Microscopy

Fluorescence microscopy images were taken 6 h post induction in a 96-well plate mounted on the stage of a Nikon Eclipse Ti microscope equipped with a 100x oil objective. α-Syn was imaged in the YFP channel. Z stacks were acquired at 0.25-μm intervals, and the resulting images were merged to maximum intensity projections in ImageJ. Cells with and without visible inclusions were counted manually in ImageJ. At least 95 cells were counted in each of three fields of view, and the results were averaged and tested for significance by one-way ANOVA adjusted for multiple comparisons. Imaging was conducted in at least biological triplicate, except for α-Syn-expressing Δ*pah1*, *pah1*-D398E, and *pah1*-7D/E, which were each evaluated once. For these latter strains, three or four different fields of view were used for statistical testing. The α-Syn-expressing Δ*nem1* and α-Syn strains were stained with Nile red using a final concentration of 0.5 μg/mL. After 5 min incubation at 30 °C, cells were washed with PBS before live cell imaging. Nile red staining was imaged in the RFP channel.

For assessment of co-localization and quantification of Nile red intensity, three regions of interest (ROI) from three fields of view per biological replicate were used as input for a co-localization pipeline in CellProfiler. Nile red and YFP channels were measured across the entire ROI with a threshold of 15% of maximum intensity and reported normalized covariance (Pearson r). To quantify lipid abundance, objects were identified in images with a diameter range of 20-100 pixels. An average of 252 Nile red positive objects and 409 YFP-positive objects were found per biological replicate. Three biological replicates were assessed for α-Syn and α-Syn Δ*nem1* samples, and two biological replicates were tested for α-Syn *pah1*-7A. A module was added to the pipeline in order to measure the Nile red intensity only within areas enclosed by Nile red-positive objects. The integrated intensity of the sum of pixel intensities within an object (arbitrary units) was used for quantification. Pearson r and integrated intensity values were averaged across all ROIs and images within each biological replicate of a given sample.

Quantification of α-Syn Abundance

α-Syn abundance in α-Syn-expressing Δ*nem1*, *pah1*-WT, and *pah1-7A* yeast was assessed by western blot (anti-α-Syn, ab27766, Abcam), and equal loading of total protein was confirmed by Ponceau staining.

Quantification of Pah1 Phosphorylation

Phosphopeptides were enriched from whole-cell lysates as described above. PRM was used to quantify 18 transitions from two phosphopeptides mapping to three known Nem1-target phosphosites and 11 transitions from two phosphopeptides containing two phosphosites not targeted by Nem1. Abundances were determined using MSStats and normalized by total ion chromatogram and Pah1 protein abundance measured from protein lysates. Abundance levels were quantified by summed transition area relative to mean sum transition areas in vector sample for each peptide across biological triplicates. Mean abundances for Nem1 target and non-target phosphopeptides were compared between α-Syn and α-Syn Δ*nem1* by two-way ANOVA adjusted for multiple comparisons, n=6, alpha=0.05 in order to assess if Pah1 phosphorylation was significantly different at Nem1-target sites and at non-target sites.

Pah1 Perturbation and Rescue Assessment

Suppression or enhancement of toxicity in *PAH1* mutants and due to chemical treatments was assessed as described above for modulator rescues. Normalized biomasses were calculated by dividing raw sum biomass values for each sample by the average signal intensity for all samples per replicate in order to eliminate technical variation between replicates measured at different times. Yeast with the estradiol transcriptional regulator integrated at the *TRP* locus and α-Syn under the control of an estradiol-regulated promoter at the *LEU* locus were cultured in galactose media and induced to express α-Syn by growth in media containing 1 nM estradiol dissolved in DMSO. Vector control was treated with DMSO only. Based on a previous report (Henry et al., 2012), 75 μM inositol

was added to media in order to inhibit expression of genes involved in phospholipid biosynthesis. Propranolol was dissolved in water and spiked into cultures at 2 mM; control samples were treated with water only. The concentration of 2 mM propranolol was previously used to inhibit Pah1 in yeast (Sasser et al., 2012). Shotgun proteomics for protein and phosphopeptide abundance changes in propranolol treated α-Syn yeast versus untreated α-Syn yeast was conducted as described above except Proteome Discoverer v2.0 was used for label-free quantification. Samples were harvested for analysis 24 h post-estradiol induction of α-Syn. A fold-change cutoff of 2 and a q value $\leq$ 0.05 were used to identify regulated proteins and phosphopeptides. The corresponding proteins of regulated phosphopeptides were input into STRING v11.0 in order to find clusters of interacting proteins. A confidence threshold of 0.9 interaction score was applied, disconnected nodes were omitted and K-means clustering was set to 10.

Analysis of Interactions between α-Syn Expression and *PAH1* Mutants

We tested for interactions between the α-Syn perturbation and each *PAH1* mutation. We defined the expected effect on growth as the product of the biomass of the individual perturbations (biomass(α-Syn) * biomass(*pah1*-mutant)). This method has been used to define a neutrality function that predicts the phenotype of two non-interacting mutations (Mani et al., 2008). We then compared the actual observed phenotype of the double-perturbation (biomass(α-Syn + *pah1*-mutant) to determine if it was significantly different than the expected phenotype.

Suppression of Toxicity by Propranolol in Mammalian Neuroblast Cells

N2A cells were incubated for 24 h with PBS or exogenous α-Syn fibrils (0.25 and 1 μM) produced from recombinant α-Syn as previously described (Gerez et al., 2019; Luk et al., 2012). Cells were treated with vehicle or 10 μM propranolol for 36 h, and cell viability was assessed by MTT assay (Promega). Compared to the yeast experiment, a lower dose of propranolol was used on N2A cells since yeast have a cell wall and N2A cells do not.

Suppression of Toxicity by Knockdown of Lipin Genes in Human Cells

HEK293 cells were transfected with a control siRNA (cat# D-001810-01-05, Dharmacon) or a pool of siRNAs targeting the *PAH1* orthologs, *lipin1*, *lipin2*, and *lipin3* (*LPIN1*a: cat# J-017427-09-0002, *LPIN1*b: cat# J-017427-11-0002, *LPIN2*a: cat# J-013458-09-0002, *LPIN2*b: cat# J-013458-11-0002, *LPIN3*a: cat# J-032702-07-0002, *LPIN3*b: cat# J-032702-08-0002, all from Dharmacon). After transfection, the cells were treated with exogenously produced α-Syn fibrils (1 μM). Viability was assessed by MTT assay.

The efficiency of siRNA-mediated knockdown of *LPIN* genes was assessed by RT-PCR. HEK293 cells were transfected with siRNAs, and the mRNAs of each *LPIN* gene were amplified by non-saturating PCR. *HSC70*, an unrelated mRNA, was used as a loading control. For RT-PCR, total RNA was isolated from the cells using RNeasy Mini Kit following manufacturer's instructions. For reverse transcription, 1 μg of RNA was incubated for 1 h at 37° C with SuperScript II reverse transcriptase in the presence of RNaseOUT RNase inhibitor and random primers, followed by an inactivation step at 95 °C for 5 min. The obtained complementary DNA (cDNA) was used as template in a 28-cycle PCR performed with the following specific primers: human *LPIN1* fwd: TGCTGGA GAGCAGCAGAACTC; human *LPIN1* rev: TAGGGTATGAGGCTGACTGAG; human *LPIN2* fwd: CCTCTCCTCAGACCAGATCG; human *LPIN2* rev: GGAGAATCTGTCCCAAAGCA; human *LPIN3* fwd: CACTCCACCCTCCACTCCTA; human *LPIN3* rev: ACAGGTA GATGGTGGCCTTG; human *HSC70* fwd: GGAGGTGGCACTTTTGATGT and human *HSC70*: GTACGGAGGCGTCTTACAGC. Amplified products were electrophoresed in a 1.5% agarose gel and stained with SYBR Green PCR.

QUANTIFICATION AND STATISTICAL ANALYSIS

Statistical tests were performed using SafeQuant (v. 2.01), MSstats (v. 0.99), Proteome Discoverer (v. 2.0) and GraphPad Prism (v. 7.0c). Methods of quantification and statistical analysis, including which test was used, the value and meaning of n, definition of center and dispersion and precision measures are included in the figure legends and Method Details section of the corresponding experiment. Unless otherwise specified, n denotes the number of independent biological samples tested in the experiment. Data in bar and box plots are represented as mean ± Standard Deviation (SD). Significance levels are defined in the figure and table legends. No explicit methods were used to test whether the data met certain assumptions or to determine strategies for randomization, sample size estimation and inclusion or exclusion of any data. For the regression and network analyses, the statistical language R (v. 3.5.1) has been used. In particular, for the regression analysis (stability selection) the R package 'c060' (v. 0.2-4) was used, while for the network analysis and the network visualization we have used the R packages 'igraph' (v. 1.2.4) (Csardi and Nepusz, 2006), 'network' (v. 1.15) (Butts, 2008) and 'ggnetwork' (v. 0.5.1) (Briatte, 2016). All the details of the methods, including thresholds, sample size and number of variables/parameters, can be found in the Method Details and the figure legends.

DATA AND CODE AVAILABILITY

The accession number for the proteomics shotgun data reported in this paper is PeptideAtlas: PASS01407 (http://www.peptideatlas.org/PASS/PASS01407). The accession number for the proteomics PRM data reported in this paper is PeptideAtlas: PASS01409 (http://www.peptideatlas.org/PASS/PASS01409).